



Distribution and fate of microplastics from the Chesapeake Bay to the Mid-Atlantic Bight: A Lagrangian particle tracking approach

Julia Abrao Teixeira^{a,*}, Piero L.F. Mazzini^a, Xun Cai^b, Manuel Colombo^a, Qubin Qin^c, Meredith Evans Seeley^a, Y. Joseph Zhang^a

^a Virginia Institute of Marine Science, William & Mary, Gloucester Point, VA, 23062, USA

^b School of the Environment, Yale University, New Haven, CT, 06511, USA

^c Department of Coastal Studies, East Carolina University, Greenville, NC, 27858, USA

ARTICLE INFO

Keywords:

Microplastic
Marine pollution
Particle tracking
Biofouling
Chesapeake Bay
Mid-Atlantic Bight

ABSTRACT

Estuaries play a critical role in mediating the flux of land-derived microplastics to the ocean, where they pose a threat to marine ecosystems. This study investigates the fate of microplastic particles exported from the Chesapeake Bay (CB) to the Mid-Atlantic Bight (MAB), using an offline Lagrangian particle-tracking approach coupled with a 3D hydrodynamic model (SCHISM). Particles were released hourly from 17 locations at the mouth of Chesapeake Bay, totaling 148,920 particles over one year. Ten sensitivity experiments were conducted, exploring how polymer type (polyethylene, polypropylene), particle size (0.001 mm, 5 mm), and biofouling influenced their distribution patterns. All scenarios showed high frequency of particles reaching Virginia and North Carolina bays. Unfouled buoyant microplastics were mainly transported southward along the Virginia and North Carolina shelves, with limited northward movement restricted to the outer shelf and offshore. When biofouling was included, particle distribution broadened and extended northward to the Gulf of Maine. As biofouled microplastics sank, interactions with cross-shelf circulation enhanced transport into inner-shelf and estuarine regions in the MAB. While polymer type had negligible effects on transport, particle size played a major role. Larger biofouled microplastics (5 mm) did not sink during the one-year simulation and followed distribution patterns similar to unfouled microplastics. Their residence time on the MAB shelf ranged between 17 and 19 days, whereas smaller biofouled microplastics (0.001 mm) had residence time nearly twice as long, between 31 and 34 days. These results underscore the importance of incorporating biofouling into predictive transport models to better assess microplastic fate in coastal systems.

1. Introduction

Marine plastic pollution has become a critical global challenge since large-scale plastic production began in the 1950s. As a consequence of low recycling rates, inadequate waste management, and widespread maritime use, a substantial proportion of plastic waste enters marine ecosystems, where it can persist for decades (Uzun et al., 2022; Lebreton et al., 2017; Pothiraj et al., 2023). Plastic production has grown exponentially, reaching 400.3 million metric tons in 2022 (Plastic Europe, 2024), with an estimated 1.5 to 12.7 million metric tons of plastic debris entering the ocean annually (Lebreton et al., 2017; Jambeck et al., 2015). Projections suggest that, even with immediate efforts to drastically reduce plastic waste, the total volume of plastic in the ocean could reach 710 million metric tons by 2040 (Arp et al., 2021), underscoring

the urgent need for coordinated global action.

A major concern within marine plastic pollution is the presence of microplastics, which are tiny plastic fragments typically ranging in size from 1 μm to 5 mm. These particles vary considerably in size, shape and chemistry (and thus, density), making them an extremely diverse contaminant class (Frias and Nash, 2019; Rochman et al., 2019). Microplastics enter the marine environment through several pathways, including riverine and coastal runoff, atmospheric deposition, and maritime activities (Andrady, 2011; Liu et al., 2019; Zhang et al., 2020). Among these pathways, land-based contributions are particularly important for microplastics, as particles may be introduced directly through runoff and wastewater effluents or formed in situ via the fragmentation of larger plastic debris (Pothiraj et al., 2023; Eriksen et al., 2014). In this context, rivers and estuaries serve as major conduits for

* Corresponding author.

E-mail address: jabraoteixeira@vims.edu (J.A. Teixeira).

transporting land-derived microplastics to the ocean, where these persistent particles can bioaccumulate, disrupt food webs, and pose significant ecological and human health risks (Akdogan and Guven, 2019; Horton et al., 2017; Browne et al., 2008; Lee et al., 2023).

Once microplastics enter the ocean, understanding their fate and distribution becomes complex. Their transport is primarily driven by physical forces such as water currents, wind, and tides (Akdogan and Guven, 2019). A key particle characteristic that drives physical fate is their buoyancy, which is dictated by material composition, density, and shape (Arp et al., 2021). Polyethylene (PE) and polypropylene (PP) are two of the most produced polymers used in many everyday items and have densities lower than that of seawater (PE: 890–980 kg/m³; PP: 830–920 kg/m³). As a result, they tend to remain buoyant and are the most prevalent microplastics detected in marine surface waters, accounting for approximately 42 % (PE) and 25 % (PP) of polymer types reported in surface samples across studies (Erni-Cassola et al., 2019; Sun et al., 2022; Van Melkebeke et al., 2020; Li et al., 2016). However, microplastics are also subject to various processes, including biofouling, aggregation with marine particles or other plastics, and fragmentation caused by photooxidation and mechanical forces. These processes can modify the initial size, density, and sometimes shape of microplastics, resulting in complex and dynamic distribution patterns within marine ecosystems (Arp et al., 2021; Chubarenko et al., 2016, 2018; Malli et al., 2022; Fazey and Ryan, 2016).

Biofouling may be a particularly important driver of microplastic fate in the ocean. This process involves the growth of microbes – including bacteria, algae and other organisms – on plastic surfaces, sometimes within days (Horton and Dixon, 2018; Jalón-Rojas et al., 2019). Biofilm development is influenced by particle surface area and environmental factors, such as nutrient availability, microbial density, temperature, and light intensity (Kooi et al., 2017). As a result of these varying factors, estimating biofilm growth rate and its effect on the sinking behavior remains highly complex, creating a notable research gap in improving microplastic fate models (Vercauteren et al., 2024). Nonetheless, environmental data underscore the importance of biofilms, as some estimates suggest that over 90 % of marine microplastics – including buoyant particles - eventually sink to the seafloor, with biofouling playing a key role in this process (Van Melkebeke et al., 2020). Using a theoretical model, Kooi et al. (2017) found that once the particles sink, they do not settle at a fixed depth but instead continuously move up and down within the water column as biofilms break down at depth and reform at the surface. This finding has also been supported empirically (Zhao et al., 2023).

A promising approach to address oceanic microplastic fate modeling is the integration of hydrodynamic numerical models with Lagrangian particle tracking. Together, these tools offer valuable insights into the movement, accumulation hotspots, residence times, and overall fate of microplastics in the marine environment, providing crucial information for microplastic control and assessment (Tsiaras et al., 2021; Sun et al., 2022; Uzun et al., 2022; Politikos et al., 2017, 2020). A novel study conducted by López et al. (2021) on the distribution of microplastics in the Chesapeake Bay – the largest estuary in the U.S. which drains a watershed that is home to over 18 million people (Moore et al., 2018) – employed numerical modeling simulations to track microplastics and understand their distribution patterns. Contrary to the common view of estuaries as sources of microplastics to the ocean, the findings indicate that Chesapeake Bay acts as a trap for riverine microplastics, allowing only positively buoyant particles to exit the bay. The authors discussed several model limitations, particularly the exclusion of remobilization of beached particles, which led to a high number of particles stranded on shorelines and likely underestimated microplastic export out of the bay. Additional limitations include deposition and resuspension of particles from the bottom, riverine inputs, model resolution, particle transformation (via biofouling and fragmentation, e.g.) and particle shape. Nonetheless, this does not change the primary conclusion that estuaries serve as a trap for many riverine-derived microplastics, while buoyant

microplastics, such as PE and PP, are more likely to reach the mouth of the Chesapeake Bay. In principle, microplastic export from the Chesapeake Bay also includes those fragmentated from large, buoyant debris at the bay mouth.

This study addresses what happens beyond the bay – how are buoyant microplastics that reach the mouth of the Chesapeake Bay transported throughout the Mid-Atlantic Bight (MAB), including the continental shelf and offshore regions? Given the ecological significance of the MAB and substantial inputs from densely populated states, understanding microplastic dynamics in this region is essential. This study employs a high-resolution numerical model to investigate transport pathways, residence times, seasonal variability, offshore export, beaching, and the role of biofouling in shaping microplastic dynamics. We address microplastics across endmember sizes: 5 mm and 1 μm. We also uniquely model the impact of biofouling, which is an important factor in highly eutrophic coastal regions, in altering particle buoyancy and fate. Ultimately, this research seeks to advance our understanding of the fate of microplastics in coastal environments, supporting improved monitoring and management strategies for the MAB and similar coastal systems.

2. Methods

2.1. Study area

The Mid-Atlantic Bight (MAB), located in the east coast of the U.S., extends nearly 1000 km along the coastline, bounded by Cape Cod (MA) to the north and Cape Hatteras (NC) to the south (Fig. 1A). Notably, the width of the MAB shelf decreases from approximately 100 km in the northern half to less than 30 km at Cape Hatteras. While moderately wide compared to other continental shelves, the MAB features a gentle bottom slope and exhibits substantial seasonal variation in stratification. It is also significantly influenced by freshwater runoff and the shelf-slope front (Lentz, 2008a,b).

The circulation on the shelf is part of a continuous coastal current stretching from Greenland to Cape Hatteras. This includes a mean equatorward along-shelf flow of 5–10 cm/s, which shifts offshore near Cape Hatteras and merges into the Gulf Stream. The strength of the along-shelf currents increases with both water depth and distance from the shore. The weakest currents are found near the New York Bight apex and south of Cape Cod, while the strongest currents are observed near the Gulf Stream, east of Cape Cod and Nantucket, and along the North Carolina coast, where a strong coastal current is present (Roarty et al., 2020; Lentz et al., 2003).

Lentz (2008) identified notable seasonal changes in the along-shelf flow, driven by variations in wind stress and the cross-shelf density gradient. The mean wind stress is approximately 0.03 N/m² toward the southeast and remains spatially uniform. However, it varies seasonally, with stronger southeastward winds in winter (0.07 N/m²) and weaker northeastward winds in summer (0.02 N/m²). These seasonal shifts in wind stress work together with the cross-shelf density gradient, which is primarily influenced by salinity differences with saltier ocean water offshore and fresher water near the coast. This salinity gradient forms as freshwater from rivers and estuaries tends to flow along the shelf as narrow buoyant currents. These buoyant currents reduce salinity on the inner shelf, intensifying the cross-shelf density gradient and enhancing the along-shelf flow. Together, these factors contribute to the seasonal variability in the along-shelf circulation.

2.2. Hydrodynamic model and particle tracking

This study employed a Lagrangian particle tracking model combined with outputs from a 3D unstructured-grid hydrodynamic model for the U.S. East Coast, developed and validated by Cai et al. (2025). The model is based on the Semi-implicit Cross-scale Hydroscience Integrated System Model (SCHISM), a derivative product built from the original SELFE

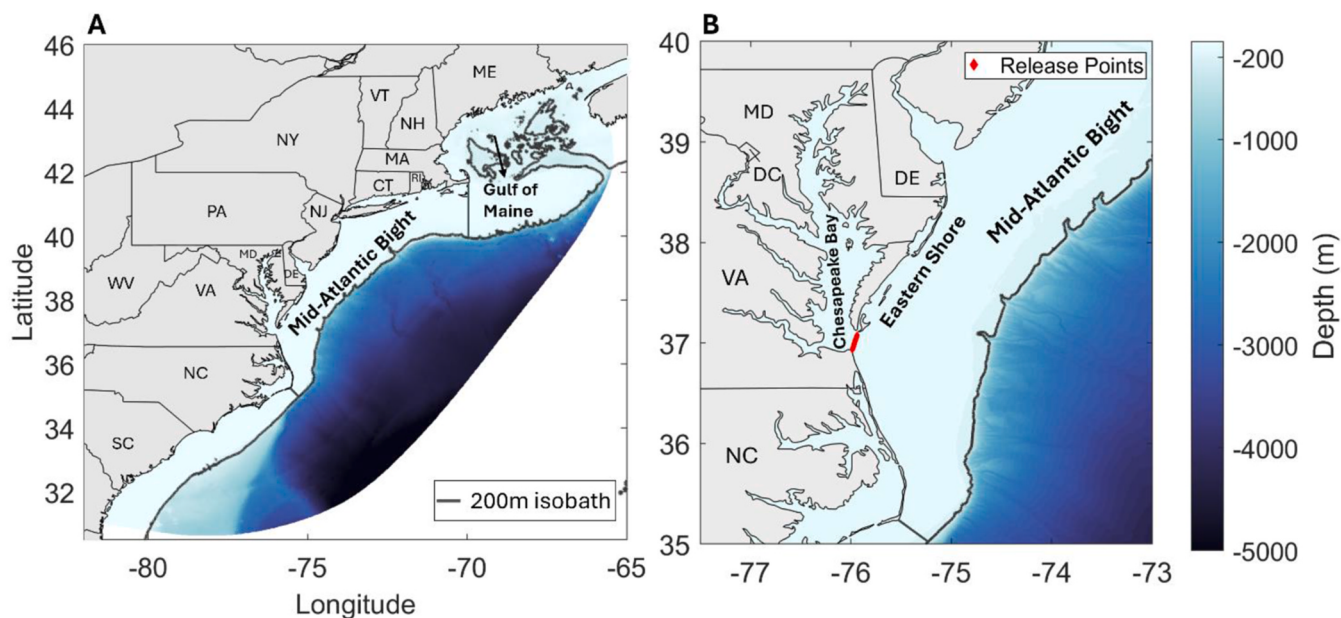


Fig. 1. (A) US East Coast grid domain (see unstructured grid in Appendix A.2). The color bar indicates depth in meters, and the continental shelf break is delineated by the 200 m isobath (thick gray contour). The Mid-Atlantic Bight region is outlined in gray. (B) Locations of particle releases at the mouth of the Chesapeake Bay, spaced approximately 1 km apart and marked by red diamonds (see zoom in Appendix A.3). (For interpretation of the references to color in this figure legend, the reader is referred to the Web version of this article.)

(v3.1dc; Zhang and Baptista, 2008), which is distributed under an open-source Apache v2 license. SCHISM has undergone numerous enhancements and upgrades, including extensions for large-scale eddying regimes and seamless cross-scale capability from creek to ocean (Zhang et al., 2016).

SCHISM employs a highly efficient and accurate semi-implicit finite-element/finite-volume method with an Eulerian-Lagrangian algorithm to solve the Navier-Stokes equations in hydrostatic form, enabling it to address a wide range of physical and biological processes. It also features a highly flexible vertical gridding system and uses an unstructured triangular-quadrangular grid in the horizontal direction (Zhang et al., 2016). A key advantage of this model, in addition to its ability to use a highly flexible grid system, is its robustness in accurately resolving complex estuarine and oceanic topography without any smoothing (Zhang et al., 2016). SCHISM's versatility has made it a widely adopted tool across various applications, from general circulation and tsunami modeling to storm-surge analysis, water quality monitoring, oil spill tracking, sediment transport, coastal ecology, and wave-current interactions, due to its diverse module integration for different environmental challenges.

The model grid used in this study (Fig. 1A) encompasses the U.S. East Coast and parts of Canadian waters. The grid consists of 983,607 elements, 540,895 nodes, and 63 vertical layers. It has a resolution of 6.5 km along the continental shelf, which is the primary area of interest for this project. River discharge data from the National Water Model (NWM; <https://water.noaa.gov/about/nwm>) was used to drive the model for the U.S. East Coast, while real-time hydrometric data (https://wateroffic.e.ec.gc.ca/map/index_e.html?type=real_time) was used for the Canadian regions. Atmospheric forcing was provided by the North American Regional Reanalysis (NARR; <https://www.ncei.noaa.gov/products/weather-climate-models/north-american-regional>), and ocean boundary conditions were defined by the Hybrid Coordinate Ocean Model (HYCOM; <https://www.hycom.org>). Tidal forcing was derived from the FES2014 database, using eight tidal constituents: M2, S2, N2, K2, K1, P1, O1, and Q1.

Hourly outputs of 3D velocity, elevation, and diffusivity were used to account for tidal effects, which can significantly influence coastal waters (Zhang et al., 2020). The simulation focused on 2013, a year selected for

its typical conditions of both discharge levels (Chesapeake Bay Activities, 2019) in Chesapeake Bay, and regional wind patterns (Appendix A.1).

The Lagrangian particle tracking model is specifically designed to simulate transport processes. In this study, we utilized SCHISM's particle tracking module ("oil spill module"), which is well-suited for representing microplastics, as it accounts for particle size, density, and beach retention. In this configuration, microplastics are modeled as individual particles, each tracked independently throughout the simulation.

The movement of each microplastic particle is driven by advection and diffusion processes. Advection is influenced by currents and the rising velocity of microplastics due to buoyancy, while diffusion accounts for the random effects of turbulent velocity. The particle tracking also incorporates the Random Displacement Model (RDM), which accurately represents particle movement by considering the effects of turbulent diffusion (Chiu et al., 2018). The particle tracking is represented as follows:

$$X^{n+1} = X^n + \left(U + \frac{\partial K_x}{\partial x} \right) \Delta t + R \sqrt{6K_x \cdot \Delta t} \quad (1)$$

$$Y^{n+1} = Y^n + \left(V + \frac{\partial K_y}{\partial y} \right) \Delta t + R \sqrt{6K_y \cdot \Delta t} \quad (2)$$

$$Z^{n+1} = Z^n + \left(W + \frac{\partial K_z}{\partial z} \right) \Delta t + R \sqrt{6K_z \cdot \Delta t} \quad (3)$$

where U, V, and W represent the water velocity components in the Cartesian coordinates x, y, and z, respectively. The variable n denotes the current time step, n + 1 indicates the next time step, and Δt is the time interval between these steps. The term R is a uniform random number ranging from -1 to 1. The K_x , K_y , and K_z correspond to turbulent diffusion coefficients in the x, y, and z directions, respectively. The horizontal diffusion coefficients were computed using the Smagorinsky model with a scaling coefficient of 0.2, typical for ocean turbulence.

Biofouling was incorporated into the particle tracking simulation

through a simplified parameterization of biofilm growth on microplastics, as proposed and implemented by Jalón-Rojas et al. (2019). This approach accounts for the progressive increase in both particle size and density resulting from biofilm accumulation, following the methodology proposed by Chubarenko et al. (2016). The density (ρ_p) of a biofouled spherical particle, considering the thickness of the biofilm layer (BT), was calculated using the following equation:

$$\rho_p = \rho_0 \frac{R_0^3}{(R_0 + BT)^3} + \rho_D \left[1 - \frac{R_0^3}{(R_0 + BT)^3} \right] \quad (4)$$

$$BT = BT_0 + BR\Delta t \quad (5)$$

where ρ_p is the density of a biofouled spherical particle (kg/m^3), ρ_0 is the density of the plastic particle (kg/m^3), R_0 is the initial microplastic radius (m), ρ_D is the density of the biofilm layer (kg/m^3), BT is the thickness of the biofilm layer (m) which is assumed to grow at a constant rate during the simulation, BT_0 is the initial biofilm thickness (m), BR is the constant biofilm growth rate (m/day), and Δt is the time interval (days).

After calculating the density of a biofouled particle ρ_p (kg/m^3), we incorporate it into the vertical velocity equation for spherical particles, as proposed by Ferguson and Church (2004) and employed by Qin et al. (2022) in their particle tracking simulations of fish egg and larval transport using the SCHISM model. The vertical velocity ω (in m/s, positive downward) is then calculated as:

$$\omega = \frac{SgD^2}{18v + (0.3|S|gD^3)^{0.5}} \quad (6)$$

$$S = \frac{\rho_p - \rho_W}{\rho_W} \quad (7)$$

$$D = 2^*(R_0 + BT) \quad (8)$$

where g is gravity (m/s^2), ρ_W is the water density (kg/m^3), D is the new microplastic diameter (initial diameter + biofilm thickness) (m), R_0 is the initial microplastic radius (m), and v is the kinematic viscosity of water ($v = \frac{\mu}{\rho_W}$), typically set to 10^{-6} (m^2/s), where μ is the dynamic viscosity (kg/(m.s)).

SCHISM's particle tracking assumes a constant ocean density of 1025 kg/m^3 and does not account for resuspension or settling. When particles sink, they are positioned 0.01 m above the seafloor to prevent them from becoming trapped, allowing continued interaction with water flow and enabling vertical movement within the water column.

2.3. Model Experiments

We selected 17 particle release points, spaced approximately 1 km apart, across the Chesapeake Bay mouth (Fig. 1B; Appendix A.3). We chose release points at the mouth, rather than from riverine sources within the Bay, to focus on particle transport as they exit the estuary and enter the MAB. Releasing particles inside the Bay would have significantly increased computational costs due to the long residence time of its waters, which averages approximately 180 days (Du and Shen, 2016).

The number of particles released in the simulations was determined based on sensitivity tests and computational efficiency. Three separate simulations were conducted to evaluate computational time and particle distribution by releasing one, two, or three particles per hour at each of the 17 release points located across the mouth of Chesapeake Bay (Fig. 1B) over the course of one year. These configurations resulted in a total of 148,920, 297,840, and 446,760 particles, respectively. Due to the substantial increase in computational time with higher particle counts, we selected the scenario with one particle per hour per release point, totaling approximately 148,920 particles annually. This approach provided a practical balance between model performance and

computational efficiency. Although the total number of particles released in this study was lower than that in López et al. (2021), the number of particles exported to the shelf is effectively higher. In their study, only 5 % of the 434,343 particles released from within the estuary were exported to coastal waters, yielding approximately 21,717 exported particles, about 15 % of the number released in the present study.

To examine how physical characteristics (e.g., density and size) and biofouling influence the distribution and fate of microplastics, we conducted a series of 10 simulations (Table 1). These included scenarios starting with a 'base case' with unfouled particles that will remain positively buoyant on the surface throughout the duration of the simulation; in this case, size is not a factor in displacement (Table 1). In addition, we also tested scenarios incorporating the effects of biofouling. Biofouled particles were also initially released at the surface but could sink over time due to increased density resulting from biofilm formation. For the biofouled particles, we considered two sizes (0.001 mm and 5 mm) and two plastic densities: 980 kg/m^3 for polyethylene (PE) and 830 kg/m^3 for polypropylene (PP).

For simulations including biofouling, given the limited data available in the literature on biofouling parameters – particularly biofilm layer density and growth rates in the MAB region – we based our parameterization on experimental values from previous studies examining biofouling on microplastic polymers. The key parameters used in equations (4) and (5) to simulate biofouling behavior are biofilm density and growth rate. For biofilm density, we applied a value of 1388 kg/m^3 (Fisher et al., 1983; Kooi et al., 2017). To explore how microplastic distribution patterns vary with biofilm growth rates, two rates are used: 6×10^{-5} mm/day, derived from bacterial and diatom colonization on plastic films (Fischer et al., 2014; Tsiaras et al., 2021), and 6×10^{-3} mm/day, empirically determined from field studies by Karkanorachaki et al. (2021). Sensitivity tests led us to apply the lower growth rate (6×10^{-5} mm/day) exclusively to particles measuring 0.001 mm in diameter, as larger particles (5 mm) would require more than one year to sink, which exceeds the median residence time of microplastic particles on the MAB shelf. The higher growth rate (6×10^{-3} mm/day) is tested across both polymer types and particle sizes. Based on the applied biofilm growth rates, the corresponding maximum biofilm thickness over a one-year simulation period is approximately 0.02 mm for the lower rate and 2.19 mm for the higher rate. In the case of the latter, this could be approximated to the formation of aggregates (e.g., marine snow) which include microplastics more than just biofouling alone, but for consistency it will be referred to as solely as biofouling hereafter.

Finally, to evaluate the influence of beaching on microplastic transport and retention, we implemented two scenarios in our simulations. In the first, we assumed that 100 % of particles reaching the land boundary became permanently stranded and did not re-enter the system. In the second, we set beaching to 0 %, allowing all particles to remain mobile within the domain. This was applied to a subset of scenarios in order to accommodate limited computational time. In SCHISM's particle tracking module, beaching is governed by a stranding algorithm that considers both boundary conditions and local cell dryness. A particle is classified as stranded when it reaches a land boundary or enters a dry area, and its presence there exceeds a minimum beaching threshold.

Although the model encompasses a larger domain, the calculations, including residence time and the number of particles exiting the region, were specifically focused on the continental shelf of the MAB (Fig. 1A, which shows the control volume). Residence time was defined as the total time a particle remained exclusively within the MAB continental shelf until it was either: exported to the deep ocean (crossing the 200-m isobath), transported to adjacent shelf regions (Gulf of Maine or South Atlantic Bight), entered and was retained within estuarine systems, or simply remained on the MAB shelf for the full simulation period (365 days). Particles retained in estuaries mark an endpoint; therefore, time spent inside estuaries is excluded from the residence time calculation to focus on shelf-specific patterns. Any time after a particle was exported to the deep ocean or adjacent shelves—including any possible return to the

Table 1

Model Experiments. Summary of simulations conducted, including the base case for unfouled positively buoyant particles, and biofouled particles for polypropylene (PP) and polyethylene (PE). The experiments account for variations in polymer densities (kg/m^3), biofouling rates (mm/day), biofouling densities (kg/m^3), particle sizes (mm), and the inclusion of beaching.

Simulation	Scenarios	Polymer Type	Initial Density (kg/m^3)	Biofouling Rate (mm/day)	Biofouling Density (kg/m^3)	Size (mm)	Beaching
1 (BASE CASE)	Unfouled	–	Positively Buoyant	–	–	–	yes
2	–	–	–	–	–	–	no
3	Biofouled	PP	830	6×10^{-5}	1388	0.001	yes
4	–	PP	830	6×10^{-3}	1388	0.001	no
5	–	PP	830	6×10^{-3}	1388	0.001	yes
6	–	PP	830	6×10^{-3}	1388	5	yes
7	–	PE	980	6×10^{-5}	1388	0.001	yes
8	–	PE	980	6×10^{-3}	1388	0.001	no
9	–	PE	980	6×10^{-3}	1388	0.001	yes
10	–	PE	980	6×10^{-3}	1388	5	yes

MAB shelf—was not included.

As the SCHISM particle tracking module does not automatically eliminate particles upon reaching the boundary, a 20 km inward buffer zone was established to exclude particles near the model edge. A 40 km buffer was also tested; however, since it did not alter the overall distribution, the 20 km buffer was considered sufficient and used in the analysis.

3. Results

3.1. Base case: Unfouled positively buoyant particles

The overall frequency of occurrence—defined as the total number of particle passages through each 5×5 km grid cell—of unfouled positively buoyant particles (i.e., Simulation 1; Table 1) for the entire simulation period (Fig. 2), is constrained approximately between latitudes 34°N and 42°N , with the peak count reaching 10^6 particles along the Virginia (VA) and North Carolina (NC) coastlines. A nearly uniform distribution of particles across the continental shelf is evident from latitude 35°N to 38°N , with a rapid decay in particle count, ranging from 10^3 to 10^0 , offshore of the shelf break for these latitudes. North of 38°N , particles are absent from the inner- and mid-shelf, instead, particle

movement is restricted to the outer-shelf and farther offshore, with a region of enhanced offshore export, reaching a particle count of 10^4 , centered around 39°N . Chesapeake Bay is the only major estuary where particles are present, particularly in its lower region likely due to tidal advection and/or estuarine gravitational circulation. The distribution of particles varies seasonally, influenced by wind direction and intensity. During winter and fall (Fig. 3A and D), unfouled positively buoyant particles exhibit a more pronounced southward movement along the inner- and mid-shelf regions off the VA and NC coasts, driven by downwelling-favorable southeastward winds that induce onshore Ekman transport in these areas. In contrast, when winds shift to upwelling-favorable conditions in spring and summer (Fig. 3B and C), particles exhibit a northward movement and a more uniform distribution across the continental shelf. Offshore, particles generally display a broader spatial distribution with enhanced latitudinal variation between seasons. A southward reach below 34°N is observed during winter and spring, while a northward reach beyond 40°N is observed in all seasons except winter. Spring shows the broadest latitudinal spread of particles, whereas summer displays the narrowest distribution.

3.2. Effects of biofouling, particle size, and particle density

The overall frequency of occurrence of biofouled particles for both polymer types, PE and PP, exhibits a similar pattern, with only minimal variations in their pathways (Figs. 4 and 5). Unlike the base case (i.e., Simulation 1; Table 1), biofouling leads to a broader dispersion of small particles (0.001 mm) both along and across the MAB continental shelf, extending between latitudes 34°N and 46°N . This pattern is observed across both biofouling rates (6×10^{-5} and 6×10^{-3} mm/day) and polymer densities for the small size class (Fig. 4A and B and 5A, B).

Similar to the base case, particles remain concentrated primarily along the VA and NC coasts, with peak counts reaching 10^6 and maintaining a similar cross-shelf distribution up to 38°N (Fig. 4A, B, C and 5A, B, C). However, biofouled particles with diameters of 0.001 mm (Fig. 4A and B and 5A, B) are now distributed further north, extending into the Gulf of Maine and spreading across the inner and mid-shelf regions of the MAB, driven by the cross-shelf circulation. These particles also enter estuaries such as Delaware Bay, the Hudson River, and Long Island Sound, with the highest particle count of 10^6 observed in Chesapeake Bay. This distribution pattern is further highlighted by the anomaly map (Fig. 6), which illustrates the difference in particle occurrence frequency between PE simulation of small biofouled particles (i.e., Simulation 9; Table 1) and the base case scenario (i.e., Simulation 1; Table 1).

However, for 5 mm particles of both PE and PP (Figs. 4C and 5C), despite the influence of biofouling, their distribution remains similar to the base case. This is because even at the highest biofouling rate, these larger diameter particles remain positively buoyant throughout the entire simulation period (one year) and therefore stay at the surface, being advected and dispersed similarly to the base case particles (i.e.,

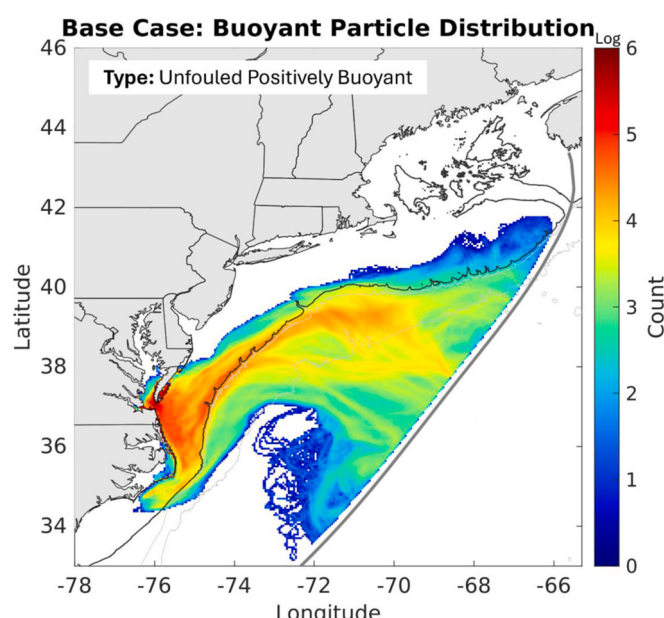


Fig. 2. Frequency of occurrence of unfouled positively buoyant particles in the base case (i.e., Simulation 1; Table 1), computed on a 5×5 km grid. Particle frequencies are shown on a \log_{10} scale. Isobaths of 200, 1000, and 3000 m are shown as gray contours, with a thicker contour denoting the 200 m isobath, highlighting the shelf break.

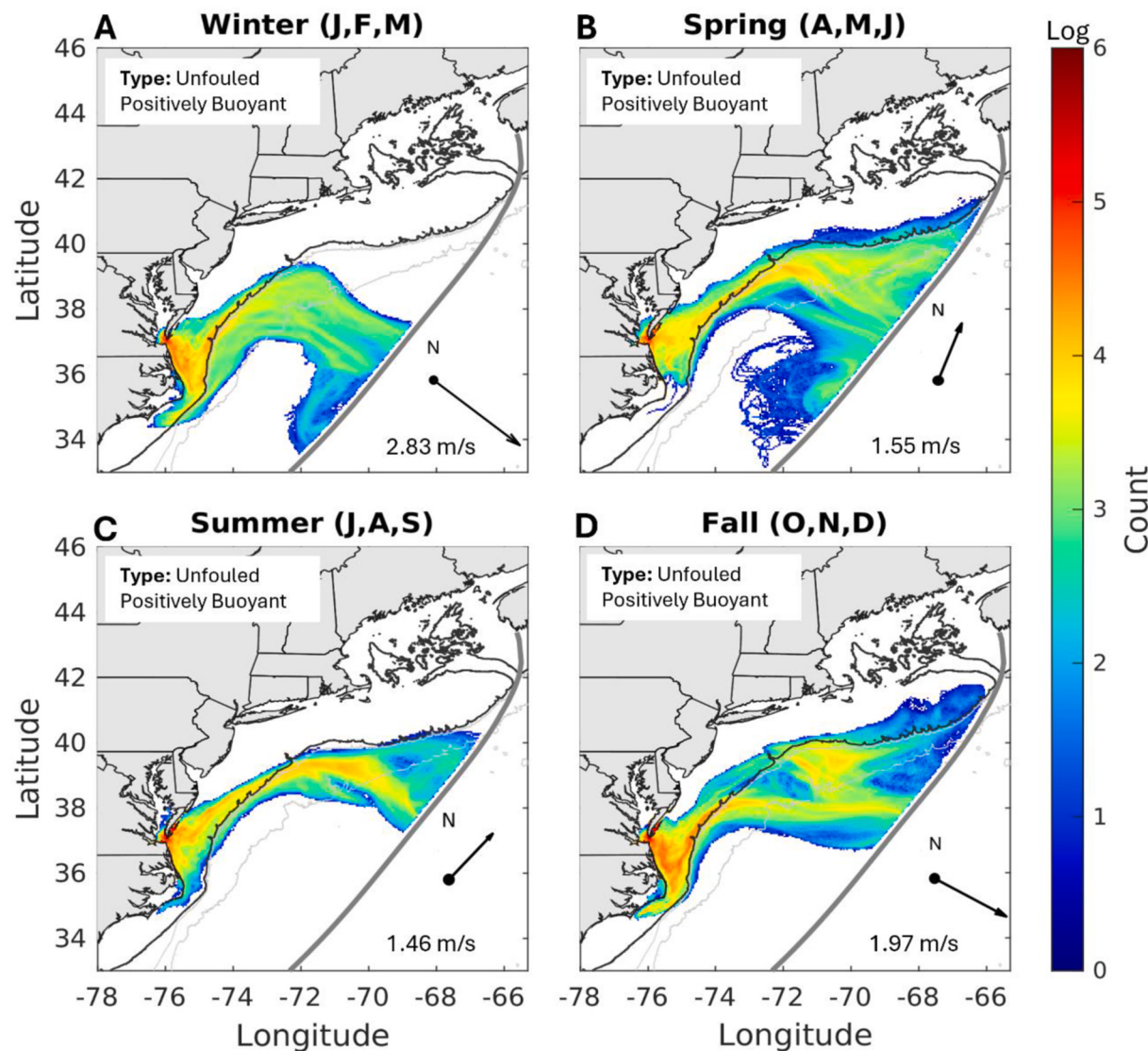


Fig. 3. Seasonal frequency of unfouled positively buoyant particles in the base case (i.e., Simulation 1; [Table 1](#)): (A) Winter (Jan, Feb, Mar), (B) Spring (Apr, May, Jun), (C) Summer (Jul, Aug, Sep), and (D) Fall (Oct, Nov, Dec) - computed on a 5×5 km grid and shown on a \log_{10} scale. Wind intensity and direction are shown by black arrows, with the mean velocity (m/s) representing both temporal averages for each season and spatial averages across the region. Isobaths of 200, 1000, and 3000 m are shown as gray contours, with a thicker contour denoting the 200 m isobath, highlighting the shelf break.

Simulation 1; [Table 1](#)).

Across all scenarios, the difference in the overall frequency of occurrence between biofouled PE and PP particles ([Figs. 4 and 5](#)) is consistently small, typically less than 2 %. Given this similarity, we focus the following discussion on Simulation 9 ([Table 1](#)), which considers biofouling only for small PE particles (980 kg/m^3 , 0.001 mm) at the highest biofouling rate of $6 \times 10^{-3} \text{ mm/day}$.

The seasonal variation in the distribution of small biofouled particles ([Fig. 7](#)) (i.e., Simulation 9; [Table 1](#)) continues to be shaped by wind direction and intensity, as observed in the base case. During winter and fall ([Fig. 7A-D](#)), particles exhibit a similar movement pattern across the continental shelf, with downwelling-favorable southeastward winds enhancing their southward transport along the VA and NC shelves. In contrast, under upwelling-favorable conditions in spring and summer ([Fig. 7B and C](#)), particles shift northward, becoming more dispersed across the shelf, reaching the Gulf of Maine, and eventually entering major estuaries in the MAB, driven by cross-shelf circulation. This seasonal pattern arises from the combined effects of seasonal wind forcing and cumulative particle transport. Upwelling-favorable winds in spring and summer enhance cross-shelf dispersion, while downwelling-

favorable winds in winter and fall constrain along-shelf transport. In fall, some particles still remain within the estuaries, likely as a result of transport that occurred earlier during the summer. Unlike unfouled positively buoyant particles (i.e., Simulation 1; [Table 1](#)), offshore particles now primarily move northward, reaching up to latitude 46°N, while southward transport beyond latitude 36°N is limited.

The vertical distribution of small biofouled particles ([Fig. 8A and B](#)) shows a tendency for them to remain, on average, within the upper 10–15 m of the water column across the continental shelf up to the latitude of 40°N, regardless of the biofouling rate. Beyond Chesapeake Bay, between latitudes 40°N and 46°N, the particles continue to sink due to biofouling, reaching greater depths of around 30 m in the northern MAB and up to 60 m in the Gulf of Maine. Further offshore, up to latitude 40°N, particles sink even deeper, becoming more concentrated near the shelf break and offshore, where depths can reach up to 250 m. When comparing the mean particle depth for PE at the same size of 0.001 mm but with different biofouling rates (i.e., Simulations 7 and 9; [Table 1](#)) the difference remains minimal, maintaining nearly identical vertical distribution patterns up to latitude 42°N, with only a slight variation observed in the Gulf of Maine.

Biofouled Particle Distribution – PE

Increasing Biofouling Rate (mm/day)

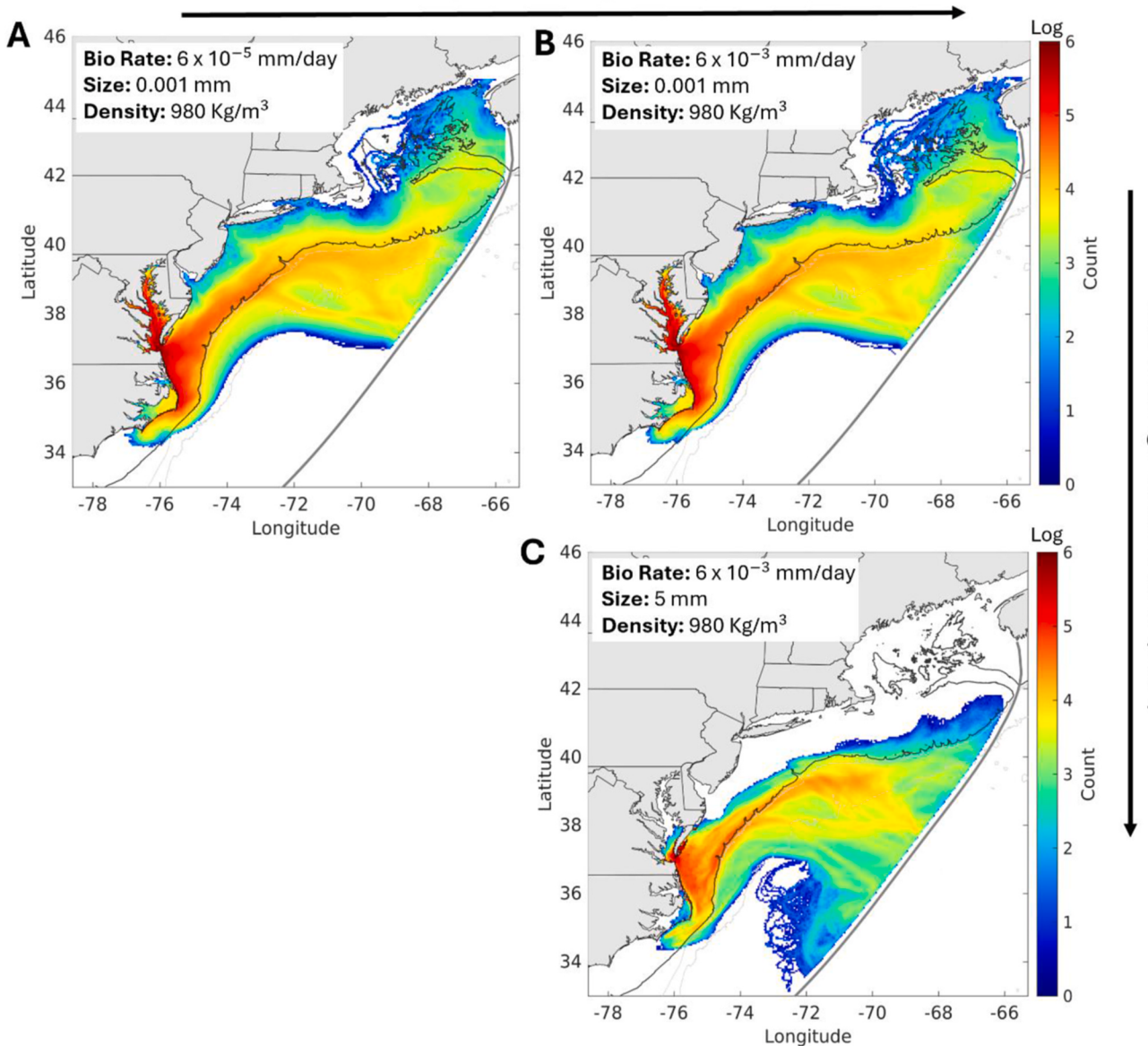


Fig. 4. Frequency of occurrence of biofouled particles computed on a 5×5 km grid with varying biofouling rates (mm/day) and particle sizes (mm) for polyethylene (PE, 980 kg/m³). (A) Biofouling rate of 6×10^{-5} mm/day and particle size of 0.001 mm (i.e., Simulation 7; Table 1); (B) Biofouling rate of 6×10^{-3} mm/day and particle size of 0.001 mm (i.e., Simulation 9; Table 1); (C) Biofouling rate of 6×10^{-3} mm/day and particle size of 5 mm (i.e., Simulation 10; Table 1). Particle frequencies are shown on a log₁₀ scale. Isobaths of 200, 1000, and 3000 m are shown as gray contours, with a thicker contour denoting the 200 m isobath, highlighting the shelf break.

3.3. Influence of beaching

The sensitivity to beaching is investigated by comparing the frequency of occurrence of unfouled positively buoyant particles in simulations with and without beaching included. The anomaly map (Fig. 9) shows the difference in particle distribution between these two scenarios. When beaching is excluded, there is a higher concentration of particles within Chesapeake Bay and Pamlico Sound, and particles are able to travel farther south. Conversely, when beaching is included, more particles become stranded along the shoreline, restricting their southward transport.

Unfouled positively buoyant (i.e., Simulation 1; Table 1) and small

biofouled PE particles (i.e., Simulation 9; Table 1) exhibit different stranding locations, with notable variations between the two scenarios (Fig. 10A and B). Unfouled particles primarily accumulate along the shorelines of VA, NC, and the Eastern Shore, as well as in the lower Chesapeake Bay, with peak particle counts of 10^4 near the bay's mouth, extending southward to latitude 36°N, where accumulation begins to decline. In contrast, small biofouled particles show greater accumulation throughout Chesapeake Bay, as well as farther south and north, with some stranding observed near Delaware Bay and the Hudson River. However, the highest particle counts, on the order of 10^4 , remain near the bay's mouth and along the VA and NC shorelines up to latitude 35.5°N, beyond which accumulation also decreases. This general trend

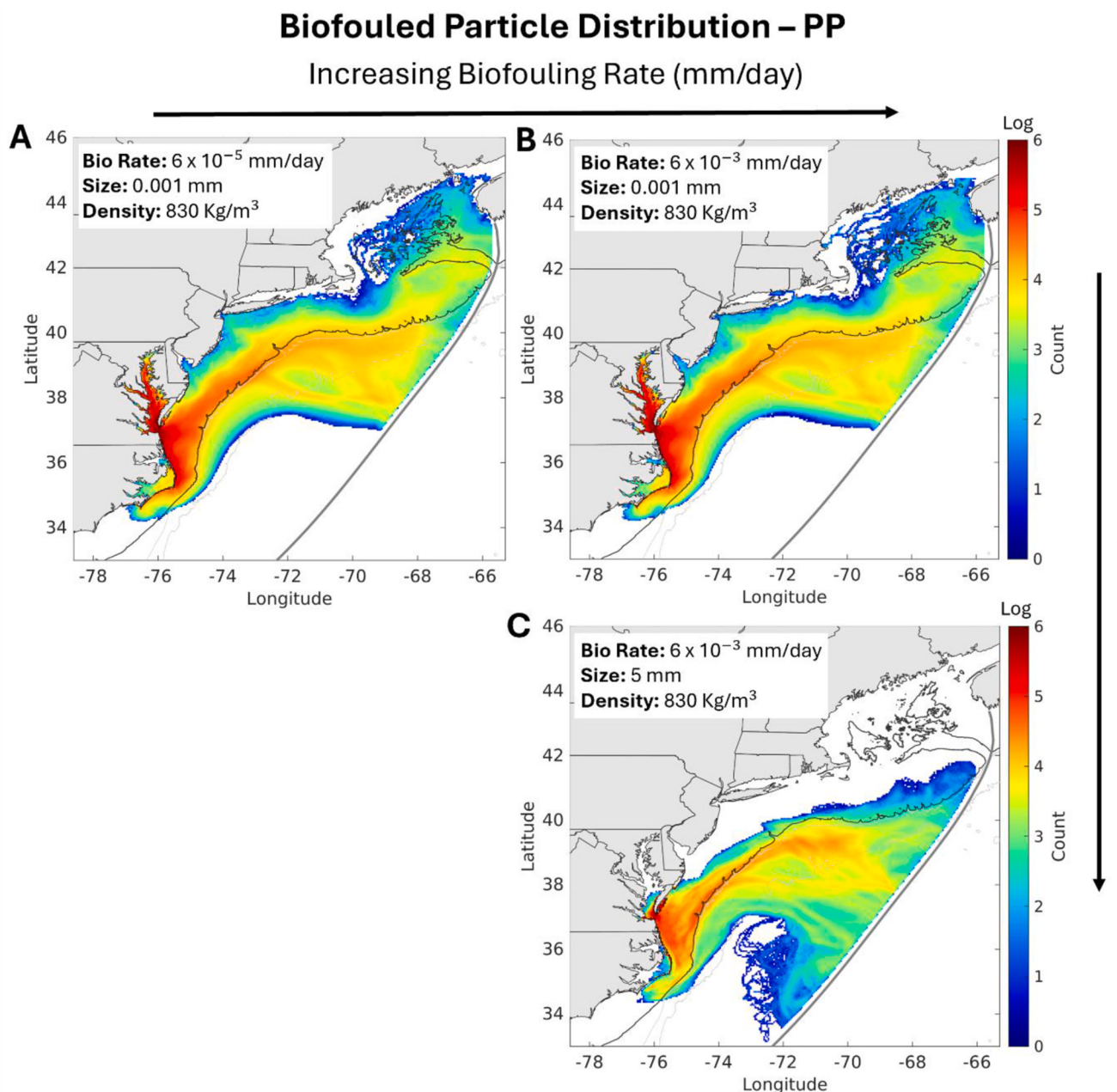


Fig. 5. Frequency of occurrence of biofouled particles computed on a 5×5 km grid with varying biofouling rates (mm/day) and particle sizes (mm) for polypropylene (PP, 830 kg/m^3). (A) Biofouling rate of 6×10^{-5} mm/day and particle size of 0.001 mm (i.e., Simulation 3; Table 1); (B) Biofouling rate of 6×10^{-3} mm/day and particle size of 0.001 mm (i.e., Simulation 5; Table 1); (C) Biofouling rate of 6×10^{-3} mm/day and particle size of 5 mm (i.e., Simulation 6; Table 1). Particle frequencies are shown on a \log_{10} scale. Isobaths of 200, 1000, and 3000 m are shown as gray contours, with a thicker contour denoting the 200 m isobath, highlighting the shelf break.

is consistent with field data from Dodson et al. (2020), who measured microplastic concentrations in beach sediments at four sites along the VA and NC coastlines. They found that fragments of both low- and high-density polymers were most abundant near the bay's mouth and decreased southward along the coast. A comparison between biofouled modeled beached particles and the measurements reported by Dodson et al. (2020) is presented in Appendix A.4, showing a strong correlation ($R = 0.98$), which indicates that the model effectively captures the large-scale beaching pattern.

Across all simulations, regardless of the polymer type, when beaching is enabled (Table 2), unfouled positively buoyant particles and 5 mm biofouled particles with the highest biofouling rate (6×10^{-3} mm/day) exhibit the highest number of beached particles. Approximately 56 % of

these particles become stranded on the shoreline, likely because they remain near the surface, facilitating the beaching process. In contrast, when biofouling is applied to 0.001 mm particles, the percentage of beached particles decreases to about 44 % at both biofouling rates (6×10^{-3} and 6×10^{-5} mm/day), likely due to the sinking behavior of smaller biofouled particles.

3.4. Residence time and particle export

Particles leaving the MAB shelf region (Fig. 1A), are primarily exported offshore through the eastern part across the shelf break in all scenarios, regardless of biofouling or polymer type (Fig. 11A and B; Table 2). Unfouled positively buoyant particles (i.e., Simulation 1;

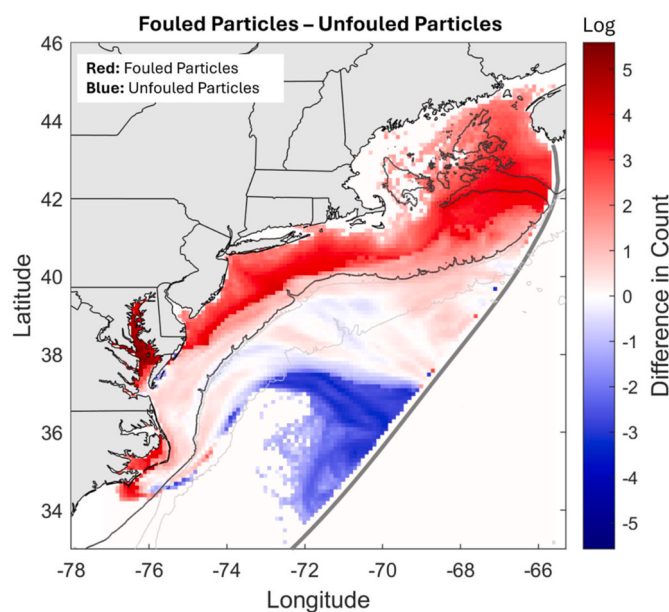


Fig. 6. Difference in distribution between small PE biofouled particles (980 kg/m^3 , 0.001 mm , biofouling rate of $6 \times 10^{-3} \text{ mm/day}$; i.e., Simulation 9; **Table 1**) and the base case for unfouled positively buoyant particles (i.e., Simulation 1; **Table 1**), calculated on $5 \times 5 \text{ km}$ grid. Red colors indicate the dominance of biofouled particles, blue colors represent the dominance of unfouled positively buoyant particles, and white colors show areas where both are present in equal amounts. Values are shown on a \log_{10} scale. Isobaths of 200, 1000, and 3000 m are shown as gray contours, with a thicker contour denoting the 200 m isobath. (For interpretation of the references to color in this figure legend, the reader is referred to the Web version of this article.)

Table 1) follow two main exit pathways: eastward and southward (**Fig. 11A**; **Table 2**). While the eastward exports occur steadily throughout the year, with 37.16 % of particles leaving the MAB, downwelling-favorable winds in winter (January to March) and fall (October to December) enhance southward transport, resulting in an export of 6.48 %. In comparison, small biofouled particles (i.e., Simulation 9; **Table 1**) follow a similar pattern (**Fig. 11B**), with 30.29 % exported eastward. However, they exhibit a stronger southward export, with 17.68 % leaving the region through the southern MAB by March, likely influenced by the same seasonal wind patterns. Unlike unfouled positively buoyant particles, a small fraction of biofouled particles (1.23 %) begin to exit the region through the northern MAB by June, after being transported into that area. Notably, a higher percentage of biofouled particles remain within the MAB, either afloat on the shelf (16.97 % for biofouled vs. 6.62 % for unfouled) or retained in estuarine systems (8.45 % for biofouled vs. 5.27 % for unfouled), supporting the observation that biofouling increases the residence time of smaller particles on the shelf.

Residence times on the MAB shelf (not including beaching or time in estuaries) vary across all simulated scenarios, depending on particle characteristics and simulation parameters (**Table 1**). Unfouled positively buoyant particles without beaching (i.e., Simulation 2; **Table 1**) exhibit a median residence time on the MAB shelf of about 19 days (**Fig. 12**), whereas including beaching (i.e., Simulation 1; **Table 1**) reduces the residence time to 17 days. Comparing polyethylene (PE) and polypropylene (PP) under biofouling conditions shows that polymer type does not significantly affect residence time. For small particles (0.001 mm) with a high biofouling rate ($6 \times 10^{-3} \text{ mm/day}$), the median residence time is 34 days without beaching (i.e., Simulations 4 and 8; **Table 1**) and decreases to 31 days when beaching is considered (i.e., Simulations 5 and 9; **Table 1**). In contrast, larger particles (5 mm) with high biofouling have a shorter median residence time of 17 days, regardless of polymer type (i.e., Simulations 6 and 10; **Table 1**). Finally,

small particles (0.001 mm) with a low biofouling rate ($6 \times 10^{-5} \text{ mm/day}$) have a median residence time of approximately 31 days (i.e., Simulations 3 and 7; **Table 1**), similar to that of small particles with high biofouling and beaching.

4. Discussion

4.1. Key findings

This study employed a hydrodynamic model coupled with Lagrangian particle tracking to investigate the pathways and fate of microplastics exported from Chesapeake Bay to the MAB shelf and offshore. We assess the influence of biofouling, particle density, size, and beaching on the spatial distribution, seasonal variability, and residence time of microplastics in the MAB shelf and surrounding regions. Model simulations revealed that biofouling plays a key role in altering small-sized microplastic pathways. Unfouled positively buoyant particles (i.e., Simulation 1; **Table 1**) were mostly confined to the southern and central portion of the MAB (between $\sim 34^\circ\text{N}$ and 42°N), showing minimal transport into the inner and mid-shelf regions north of the Chesapeake Bay as a result of surface wind-driven currents advecting the particles offshore. In contrast, once small microplastics sank due to biofouling, they were influenced by subsurface currents, spreading them more broadly along and across the shelf, reaching inner shelf regions, estuaries, and extending as far north as the Gulf of Maine ($\sim 46^\circ\text{N}$). Despite differences in their distribution in the northern portion of our study region, both buoyant and sinking particles showed consistent southward transport along the VA and NC coasts, with a uniform cross-shelf distribution up to the northern limit of Chesapeake Bay ($\sim 38^\circ\text{N}$). The high frequency of occurrence observed in these areas is likely driven by the strong coastal currents along the VA and NC coastlines ([Mazzini et al., 2019](#)). Seasonal maps of surface, subsurface, and near-bottom currents, included in [Appendix A.5, A.6, and A.7](#), further illustrate these patterns and help explain the observed differences in particle transport under varying flow conditions.

In the presence of active biofouling, our results show that particle size was the primary factor influencing microplastic distribution, rather than polymer type (PE and PP) or biofouling rate. Particle size affects how quickly biofouling alters a particle's effective density, which determines whether it sinks or stays afloat. Even at higher biofouling rates, larger particles (5 mm) did not reach negative buoyancy during the one-year simulation and exhibited surface transport patterns similar to those of unfouled particles in the base case. In contrast, smaller particles (0.001 mm) increased density more quickly, sank, and followed broader dispersal pathways influenced by subsurface currents, unlike unfouled positively buoyant particles, which remained at the surface and exhibited more limited movement. In the case of small particles being biofouled at high rates, this process is more akin particle agglomeration with other organic matter (e.g., marine snow) as a particle this small would not support a true 'biofilm'. Nonetheless, this underlines the key role that incorporation with natural organic matter can play in the transport of microplastics.

4.2. The role of biofouling in shaping microplastic pathways

Predicting the transport and fate of microplastics in marine environments is inherently complex due to the wide range of particle sizes and densities ([Frias and Nash, 2019](#)), and intricate biogeochemical processes (e.g., biofouling, remineralization of organic material) affecting their distributions. Although low-density polymers such as PE and PP – which constitute the majority of global plastic production – are initially positively buoyant, studies have suggested that over 90 % of marine microplastics may ultimately sink to the seafloor ([Van Melkebeke et al., 2020](#)). This apparent contradiction highlights the crucial role of biofouling in reducing particle buoyancy and enabling vertical transport within the water column ([Kooi et al., 2017](#); [Amaral-Zettler](#)

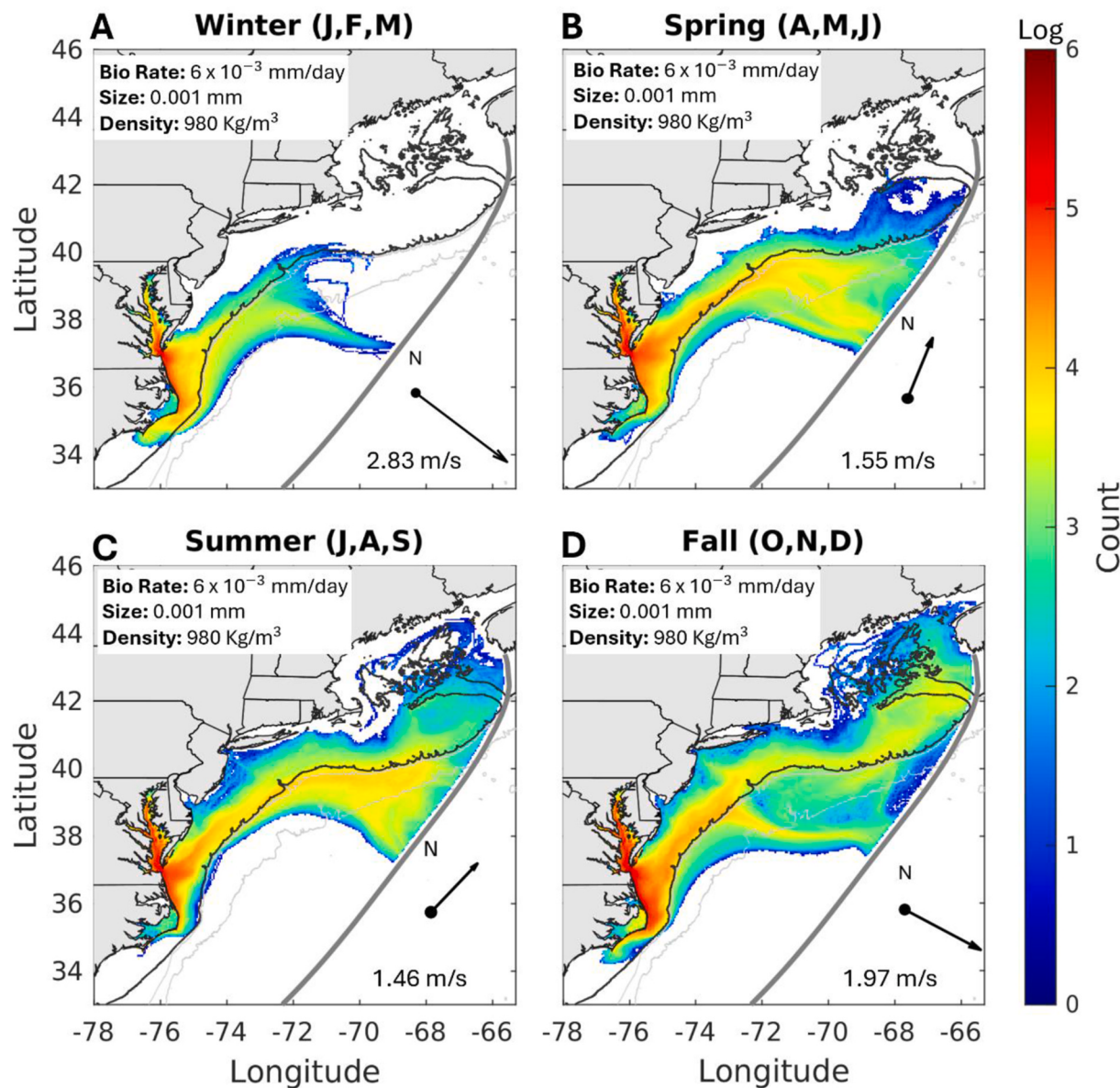


Fig. 7. Seasonal frequency of PE biofouled particles (980 kg/m^3 , 0.001 mm , biofouling rate: $6 \times 10^{-3} \text{ mm/day}$; i.e., Simulation 9; [Table 1](#)) during (A) Winter (Jan, Feb, Mar), (B) Spring (Apr, May, Jun), (C) Summer (Jul, Aug, Sep), and (D) Fall (Oct, Nov, Dec) - computed on a $5 \times 5 \text{ km}$ grid and shown on a \log_{10} scale. Wind intensity and direction are shown by black arrows, with the mean velocity (m/s) representing both temporal averages for each season and spatial averages across the region. Isobaths of 200, 1000, and 3000 m are shown as gray contours, with a thicker contour denoting the 200 m isobath, highlighting the shelf break.

[et al., 2021](#); [Karkanorachaki et al., 2021](#)).

Although several studies have modeled microplastic pathways in estuarine and coastal regions using particle tracking models ([López et al., 2021](#); [Cohen et al., 2019](#); [Sousa et al., 2021](#); [Gorman et al., 2020](#); [Zhang et al., 2020](#)), only a limited number of studies have considered the sinking behavior induced by biofouling ([Tsiaras et al., 2021](#); [Besseling et al., 2017](#); [Lobelle et al., 2021](#)), and therefore little is still known about their influence on microplastic fate in these areas. To address this, the present study incorporates vertical movement due to biofouling into the particle tracking model, using a simplified parameterization of biofilm growth by progressively increasing the size and density of microplastic particles, as proposed by [Jalón-Rojas et al. \(2019\)](#).

Our results demonstrate that biofouling plays a critical role in shaping the distribution of small-sized microplastics by allowing particles to sink and interact with subsurface currents. When biofouling is included in the simulations, smaller microplastic particles spread more widely along the coast, reaching as far north as the Gulf of Maine. During

upwelling events, particularly in spring and summer, onshore subsurface currents advect small biofouled particles to the inner and mid-shelf regions of the central and northern portions of the MAB, directing them into estuaries such as Chesapeake Bay, Delaware Bay, the Hudson River, and Long Island Sound. The distribution of small biofouled particles contrast sharply with the base case (i.e., Simulation 1; [Table 1](#)), in which unfouled positively buoyant particles remain at the surface and are primarily concentrated in the southern and central portions of the MAB, as well as in offshore regions. The equatorward mean shelf circulation ([Lentz, 2008a,b](#)) drives most particles located over the continental shelf southward, and this along-shelf flow limits the presence of buoyant particles in the inner and mid-shelf regions north of the Chesapeake Bay. As a result, small biofouled particles exhibit nearly twice the residence time on the MAB shelf compared to buoyant particles, largely due to their interaction with cross-shelf dynamics, including landward transport during upwelling. These findings highlight the critical role of sinking behavior in enhancing the retention of microplastics in coastal

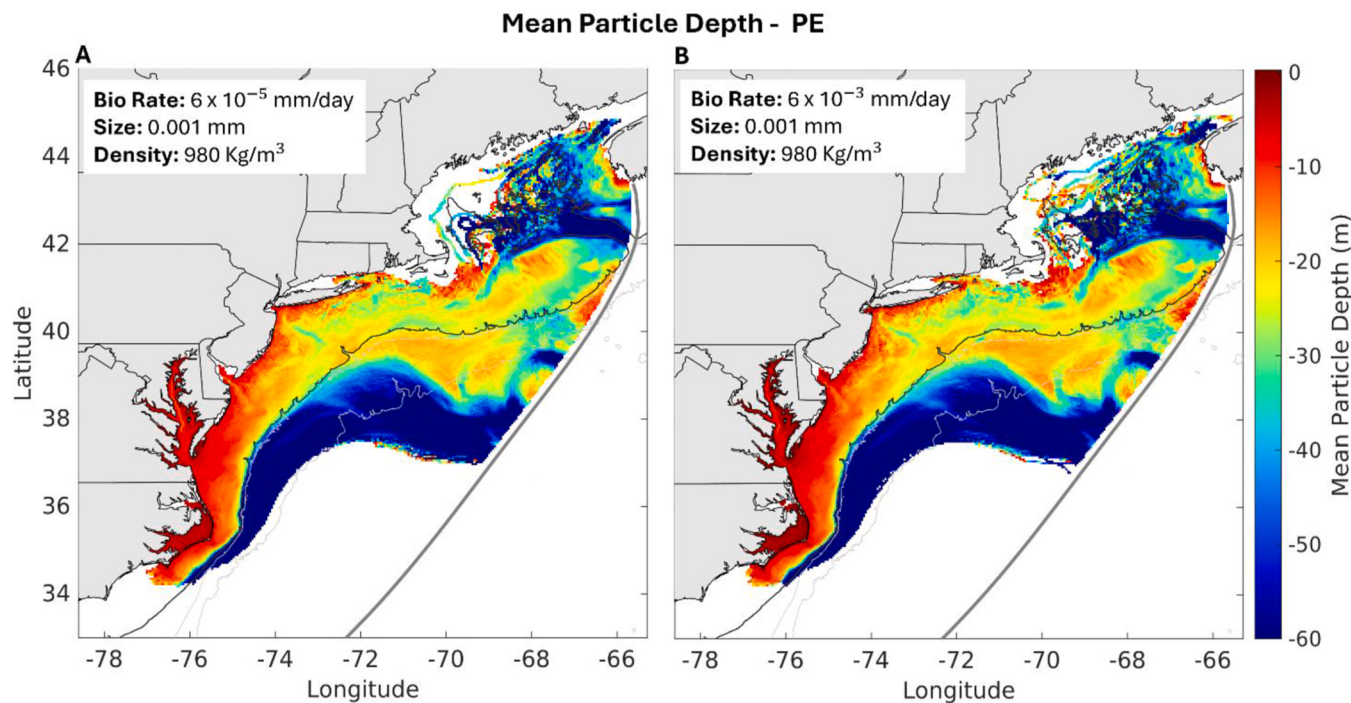


Fig. 8. Mean depth of small PE (980 kg/m^3 , 0.001 mm) biofouled particles, computed on a $5 \times 5 \text{ km}$ grid (A) biofouling rate: $6 \times 10^{-5} \text{ mm/day}$ (i.e., Simulation 7; Table 1); and (B) $6 \times 10^{-3} \text{ mm/day}$ (i.e., Simulation 9; Table 1). The colormap was limited to the maximum depth of 60 m for better visualization of particles in shallower areas, although offshore particles can reach depths of up to 250 m. Isobaths of 200, 1000, and 3000 m are shown as gray contours, with a thicker contour denoting the 200 m isobath, highlighting the shelf break.

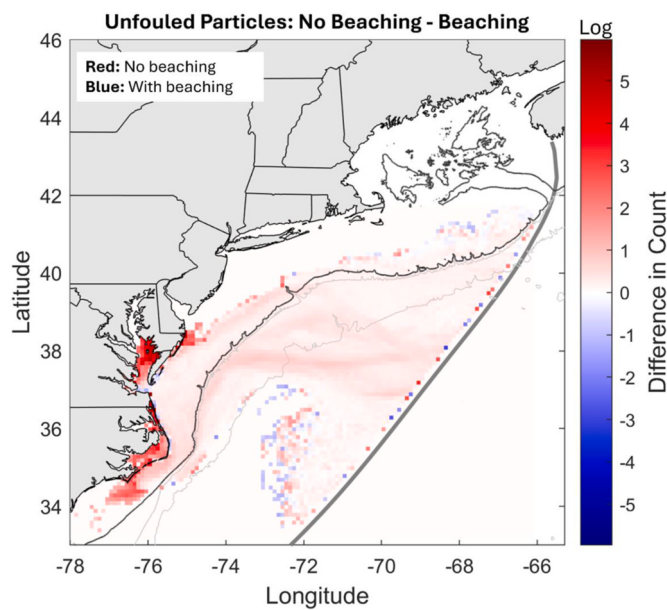


Fig. 9. Difference in particle distribution on a grid of $5 \times 5 \text{ km}$ between the base case of unfouled positively buoyant particles without beaching and the simulation including beaching (i.e., Simulations 2 and 1; Table 1). Red colors indicate the dominance of particles without beaching, blue colors indicate the dominance of particles with beaching, and white colors show areas where both are present in the same amount, regardless of beaching. Values are shown on a \log_{10} scale. Isobaths of 200, 1000, and 3000 m are shown as gray contours, with a thicker contour denoting the 200 m isobath, highlighting the shelf break. (For interpretation of the references to color in this figure legend, the reader is referred to the Web version of this article.)

and estuarine environments.

While microplastic particles exhibited distinct distribution patterns under biofouling conditions compared to unfouled positively buoyant particles, both scenarios showed a high frequency of occurrence along the Virginia and North Carolina coasts. This suggests that, after being exported from the Chesapeake Bay, particles are initially transported southward by a strong coastal current along the Virginia and North Carolina coasts (e.g. Mazzini et al., 2019), following the predominant equatorward along-shelf circulation in the MAB (Lentz, 2008a,b). As they approach Cape Hatteras, their trajectory shifts offshore, eventually merging into the Gulf Stream, leading to a large net export of shelf waters to the deep ocean (Seim et al., 2022). This pathway likely explains why particles, regardless of buoyancy, do not extend south of latitude 34°N . Once offshore, their transport is primarily governed by the Gulf Stream.

Overall, the shift in distribution between small biofouled and unfouled positively buoyant particles demonstrates how biofouling and natural organic matter agglomeration fundamentally alters microplastic pathways, enabling particles to travel farther within coastal regions and increasing their likelihood of interacting with sensitive inner-shelf and estuarine habitats. Notably, small biofouled particles released from a single estuary, such as Chesapeake Bay, can reach other estuaries and even the Gulf of Maine. This highlights the potential for microplastics to cross state boundaries and underscores the need for coordinated interstate efforts in mitigation and monitoring. Incorporating biofouling into future modeling and monitoring plans is essential to improve predictions of microplastic transport and accumulation in coastal systems.

4.3. Refining ocean plastic pathways using 3D modeling

Understanding microplastic pathways remains highly challenging due to the interplay of numerous physical and biogeochemical processes, which lead to complex distribution patterns in marine environments (Arp et al., 2021; Chubarenko et al., 2016, 2018; Malli et al., 2022; Fazey and Ryan, 2016). These challenges are further aggravated

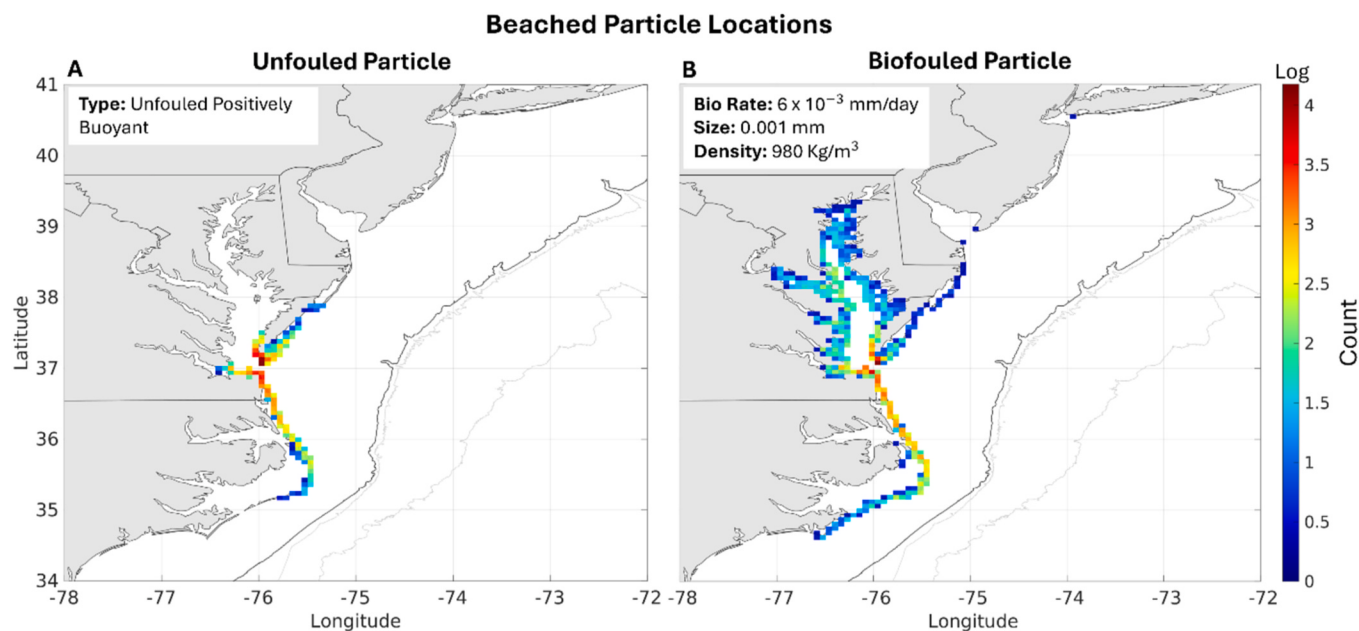


Fig. 10. Beached particle locations for (A) unfouled positively buoyant particles (i.e., Simulation 1; Table 1) and (B) small biofouled PE particles (PE – 980 kg/m³, 0.001 mm, 6×10^{-3} mm/day; i.e., Simulation 9; Table 1). The particle frequency was calculated on a 7 × 7 km grid to improve the visualization of areas where particles tend to become stranded. Results are shown on a log₁₀ scale. Isobaths of 200, 1000, and 3000 m are shown as gray contours, with a thicker contour denoting the 200 m isobath, highlighting the shelf break.

Table 2

Particle Fate. Summary of particle fate outcomes for unfouled positively buoyant particles (i.e., Simulation 1; Table 1) and small, highly biofouled PE particles (PE – 980 kg/m³, 0.001 mm, 6×10^{-3} mm/day; i.e., Simulation 9; Table 1) released in the MAB. Values represent the percentage of particles that became beached anywhere within the model domain (Fig. 1A), remained in the MAB (either beached on the shelf or remained afloat on the shelf), or exited the MAB through specific boundaries (East at 200 m isobath, South at 35°N, North at 70°W, or were retained in estuaries). Percentages are calculated relative to the total number of particles released in each simulation.

Particle Fate	Unfouled Particle	Biofouled Particle
Total model domain		
Beached particles	56.15 %	44.27 %
Staying in the MAB		
- Beached in MAB	44.47 %	25.38 %
- Afloat on shelf	6.62 %	16.97 %
Leaving the MAB		
- East (200m)	37.16 %	30.29 %
- South (35°N)	6.48 %	17.68 %
- North (70°W)	0 %	1.23 %
- Retained in estuaries	5.27 %	8.45 %

by limited observational data and the complexities of ocean circulation, making it difficult to accurately predict microplastic transport. A promising approach to address these limitations is the use of hydrodynamic numerical models coupled with Lagrangian particle tracking techniques. As demonstrated in this study, this modeling framework allows for a more detailed understanding of microplastic dynamics by simulating their three-dimensional movement, identifying distribution patterns, estimating residence times, and assessing their potential fate in the marine environment. Such tools are increasingly recognized for their value in refining ocean plastic budgets and informing strategies for pollution monitoring and management (Tsiaras et al., 2021; Sun et al., 2022; Uzun et al., 2022; Politikos et al., 2017, 2020; Lobelle et al., 2021).

This research provides valuable insights for enhancing monitoring programs by identifying transport pathways influenced by particle properties (e.g. size, density) and vertical transport processes driven by

biofouling. The simulation results are crucial for guiding field surveys by highlighting likely microplastic pathways and beaching zones across the MAB, Gulf of Maine, and adjacent estuarine environments. Stranding of both unfouled positively buoyant and biofouled particles was observed along the coasts of VA, NC, the Eastern Shore, and within Chesapeake Bay. While unfouled positively buoyant particles primarily strand in the lower Chesapeake Bay, small biofouled particles display a broader spatial distribution throughout the Bay and also strand in areas such as Delaware Bay and the Hudson River. The consistent distribution patterns identified in all scenarios, where unfouled positively buoyant particles are transported by surface currents and small biofouled particles are influenced by subsurface currents, provide essential insights for the development of targeted and effective monitoring and management strategies in both coastal and offshore regions.

4.4. Modeling limitations

This section outlines key limitations of the particle tracking model setup and the parameters used to simulate microplastic distribution. These include the number of particles released, the treatment of beaching, and uncertainties in biofouling-related parameters, such as biofilm growth rate and the density of the biofilm layer. While addressing these limitations in more detail could improve the model's accuracy in representing real-world conditions, doing so would require additional data beyond the scope of this study. Nevertheless, the simulations were specifically designed to assess the sensitivity of microplastic distribution to key factors such as polymer type (PE vs PP), particle size, biofouling with varying biofilm growth rates, and beaching. By exploring the sensitivity of these factors, the results presented in this study provide valuable insights into how key parameters influence the fate and transport of microplastics in the marine environment.

One specific limitation concerns the particle release assumptions. The model employs a constant release rate and does not account for temporal variations in microplastic input associated with streamflow. The Chesapeake Bay receives a mean annual freshwater discharge of approximately 2500 m³/s (Goodrich, 1988), and it is well established that microplastic concentrations increase during rainfall and storm

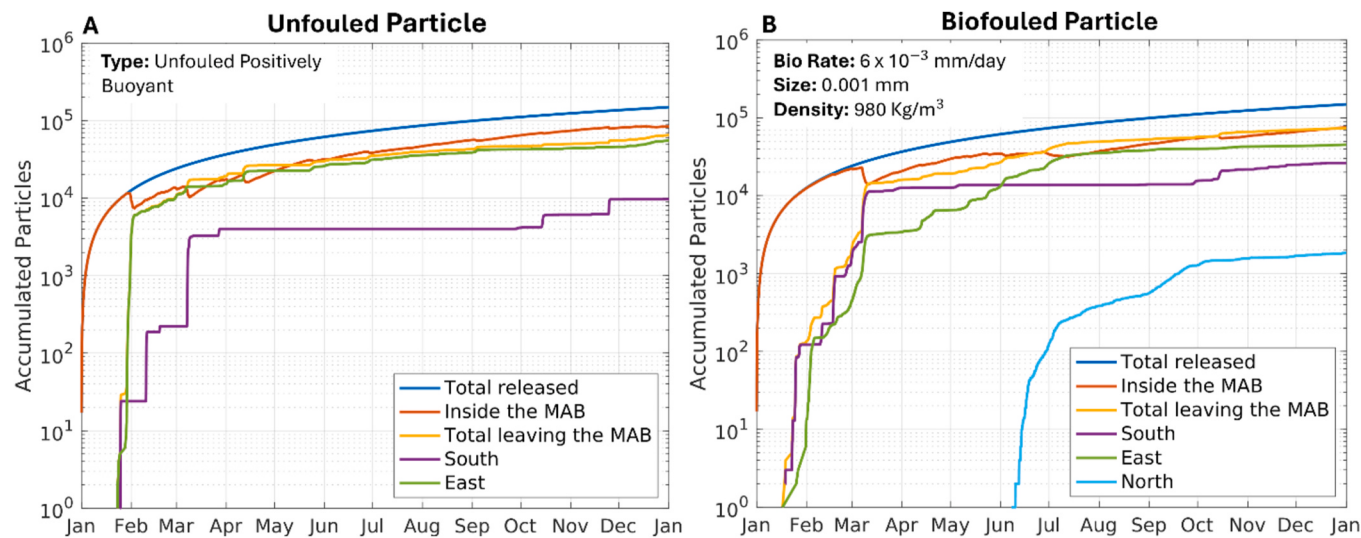


Fig. 11. Fraction of total particles released shown in dark blue, with the fraction remaining within the MAB (beached + afloat) shown in orange and those exiting the MAB in yellow. For exiting particles, the direction of exit—toward the southern (purple), eastern (green), or northern (light blue) boundaries of the MAB region—is indicated (see Fig. 1A). Results are shown for both unfouled positively buoyant particles (i.e., Simulation 1; Table 1) – none of which exit through the north (A) and small, highly-biofouled PE particles (PE – 980 kg/m³, 0.001 mm, 6×10^{-3} mm/day; i.e., Simulation 9; Table 1). (For interpretation of the references to color in this figure legend, the reader is referred to the Web version of this article.)

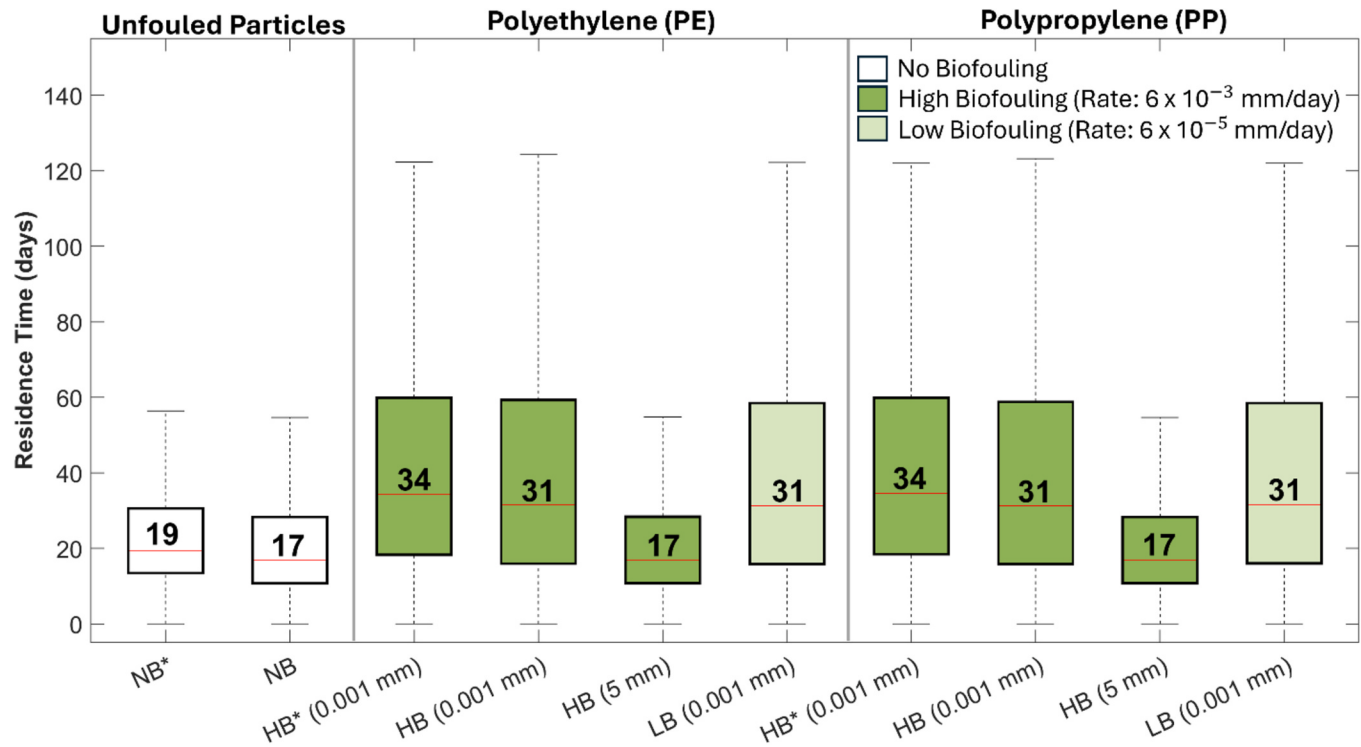


Fig. 12. Boxplots of residence time (days) in the MAB, not including time beached or entrained in estuaries, for different particle types and conditions. Unfouled positively buoyant particles are shown in white, under two scenarios: without beaching (*) and with beaching. Biofouled PE and PP particles are shown for a high biofouling rate (6×10^{-3} mm/day) and a low biofouling rate (6×10^{-5} mm/day), both applied to 0.001 mm particles. High biofouling rate scenarios are shown in dark green, and low biofouling rate in light green. For the 0.001 mm particles under the high biofouling rate condition, results are shown for both without (*) and with beaching. The 5 mm biofouled particles are also included under the high biofouling rate condition. Each boxplot displays the minimum, first quartile (Q1), median (in red), third quartile (Q3), and maximum residence time, excluding outliers. The number inside each box represents the median residence time. (For interpretation of the references to color in this figure legend, the reader is referred to the Web version of this article.)

events due to enhanced runoff and transport, especially in densely populated watersheds (Hitchcock, 2020; Yonkos et al., 2014). Incorporating real-time variability in particle concentrations was not feasible in this study due to the limited availability of observational data in the

region.

A significant limitation of the current model is the absence of surf zone and wave dynamics, which leads to an overestimation of the beaching process. Following the methods used in this study (Section

2.3), all particles reaching the land boundary are assumed to become permanently stranded, without accounting for potential remobilization by waves, wind, tides, or runoff. The model also does not include wave-driven transport mechanisms such as Stokes drift, which is known to influence the transport of floating particles (Isobe et al., 2014; Iwasaki et al., 2017; Jalón-Rojas et al., 2025). In wave-dominated environments, highly buoyant particles tend to remain near the surface and are transported onshore with the waves. Particles with lower rising velocities are more affected by turbulent mixing and can become distributed throughout the water column, while high-density microplastics often accumulate near the breaking zone (Jalón-Rojas et al., 2025). Future studies should aim to improve the representation of these coastal processes to better capture the beaching behavior and nearshore dynamics of microplastic particles.

A key limitation of this study is how biofouling is simulated. Modeling the effects of biofouling on microplastic particles is highly complex, as biofilm formation can be influenced by a variety of environmental factors, including nutrient availability, dissolved oxygen, temperature, light intensity, and the type and size (particularly surface area) of the microplastic particles themselves (Chiu et al., 2005; Costerton, 1995; Kooi et al., 2017; Karkanorachaki et al., 2021). These factors can influence the biofilm growth rate, introducing significant uncertainties in estimating this rate over time and its subsequent impact on sinking behavior. As a result, this complexity poses challenges in making precise predictions regarding the movement of microplastics in marine environments (Vercauteren et al., 2024).

Given these challenges and the lack of data on biofouling formation on microplastic particles, especially in the MAB region, the simulation was based on a simplified parameterization of microplastic biofilm growth, as proposed by Jalón-Rojas et al. (2019). We based our parameterization on experimental values from previous studies examining biofouling on microplastic polymers (Fischer et al., 2014; Karkanorachaki et al., 2021; Fisher et al., 1983). The parameters used in the simulation, particularly the wide range of biofouling growth rates (outlined in Section 2.3, Model Experiments), allow us to gain valuable insights into microplastic distribution under different conditions. These data were largely empirically derived from larger plastics or plastic films, not from small microplastics as we modeled here. Therefore, the growth rate likely exceeds what is reasonable biofilm growth for a small microplastic (1 μm, as modeled here), but could be considered a model of particle agglomeration with biological material (e.g., marine snow or particulate organic matter) over time. Moreover, our models did not allow for decreases in biofilm growth over time or mineralization of the biofilm at depth, both of which are likely important in driving the fate of microplastics. Nonetheless, the models presented here serve as a foundation to explore the extreme scenarios in microplastics offshore distribution – from the smallest to the largest microplastics, and none or extreme biofouling.

While addressing the limitations outlined in this section could lead to more accurate and realistic results, the methods and findings of this study were designed to bridge existing gaps and provide valuable insights to inform upcoming research. Future studies should expand on this work by incorporating additional transformation processes, such as fragmentation and aggregation (highlighted as important here in the case of heavy biofouling), especially in long-term simulations. They should also examine the sensitivity of microplastic transport to wind forcing, river discharge, and currents, as these factors can strongly influence along-shelf and cross-shelf transport patterns. Furthermore, efforts should focus on generating realistic experimental data from the MAB to improve the parameterization of biofilm dynamics and enhance the accuracy of numerical models.

5. Conclusion

This study used a hydrodynamic model with Lagrangian particle tracking to investigate how microplastic movement is influenced by

polymer types (PE and PP), particle size, biofouling-driven vertical transport, residence times, and the ultimate fate of microplastics exported from Chesapeake Bay to the MAB shelf and offshore regions. The study highlights the critical role of biofouling in altering microplastic distribution by inducing sinking and advection by subsurface currents. Small biofouled particles disperse widely across the continental shelf over the entire MAB, extending into estuarine environments and into the Gulf of Maine. In contrast, particles that remain buoyant at the surface are mostly confined to the MAB shelf up to the northern limit of Chesapeake Bay (~38°N), with their movement largely restricted to the outer shelf and offshore areas beyond this point. The difference in distribution between unfouled positively buoyant and small biofouled particles underscores the importance of incorporating sinking behavior induced by biofouling in future simulation studies. Interestingly, we found that particle size, when biofouling is activated, had a stronger influence on microplastic transport patterns than polymer type (PP and PE) or the biofilm growth rate. Larger particles remained afloat throughout the simulation, as they did not accumulate enough biofilm to increase their density and sink. In contrast, smaller particles became denser more quickly, sank, and followed transport pathways distinct from those of positively buoyant particles. These findings emphasize the importance of including size-dependent sinking behavior driven by biofouling in future models to better predict microplastic movement in the ocean. Despite certain model limitations, such as beaching dynamics and simplified biofouling parameterizations, this study provides valuable insights into microplastic dynamics in the MAB and surrounding regions helping to support the development of more effective monitoring and mitigation strategies. Our results suggest that future studies should focus on refining modeling techniques, particularly by incorporating more realistic representations of biofouling processes, such as improved parameterizations of biofilm growth rates and densities based on experimental data. Additionally, accounting for other particle transformation processes, such as fragmentation and aggregation, will be critical for enhancing predictions of microplastic distribution and supporting management efforts in coastal and estuarine environments. Given the complexity of microplastic transport, incorporating these processes will provide important information to guide future surveys and improve monitoring programs in these vulnerable regions.

CRediT authorship contribution statement

Julia Abrao Teixeira: Writing – original draft, Visualization, Software, Methodology, Investigation, Formal analysis, Data curation, Conceptualization. **Piero L.F. Mazzini:** Writing – review & editing, Supervision, Funding acquisition, Conceptualization. **Xun Cai:** Writing – review & editing, Validation, Supervision, Resources, Methodology. **Manuel Colombo:** Writing – review & editing, Supervision, Conceptualization. **Qubin Qin:** Writing – review & editing, Supervision, Conceptualization. **Meredith Evans Seeley:** Writing – review & editing, Supervision, Conceptualization. **Y. Joseph Zhang:** Writing – review & editing, Supervision, Software, Methodology, Conceptualization.

Funding statement

This research was supported by the Virginia Institute of Marine Science (VIMS) through graduate student funding, and by one year of Federal funding under award [NOAA Award/Grant #NA24OARX417C0153], Virginia Sea Grant College Program Project [VASG Project #727522], from the National Oceanic and Atmospheric Administration's (NOAA) National Sea Grant College Program, U.S. Department of Commerce. The statements, findings, conclusions, and recommendations are those of the author(s) and do not necessarily reflect the views of Virginia Sea Grant, NOAA, or the U.S. Department of Commerce.

Declaration of competing interest

The authors declare that they have no known competing financial interests or personal relationships that could have appeared to influence the work reported in this paper.

Acknowledgements

The authors gratefully acknowledge the Virginia Institute of Marine

Science (VIMS) for providing graduate funding support, as well as the Virginia Sea Grant (VASG) Program Development Award (award number NA24OARX417C0153), which supported one year of this research. The authors also sincerely thank the anonymous reviewers for their valuable comments and suggestions, which helped improve the clarity and quality of this manuscript.

Appendices.

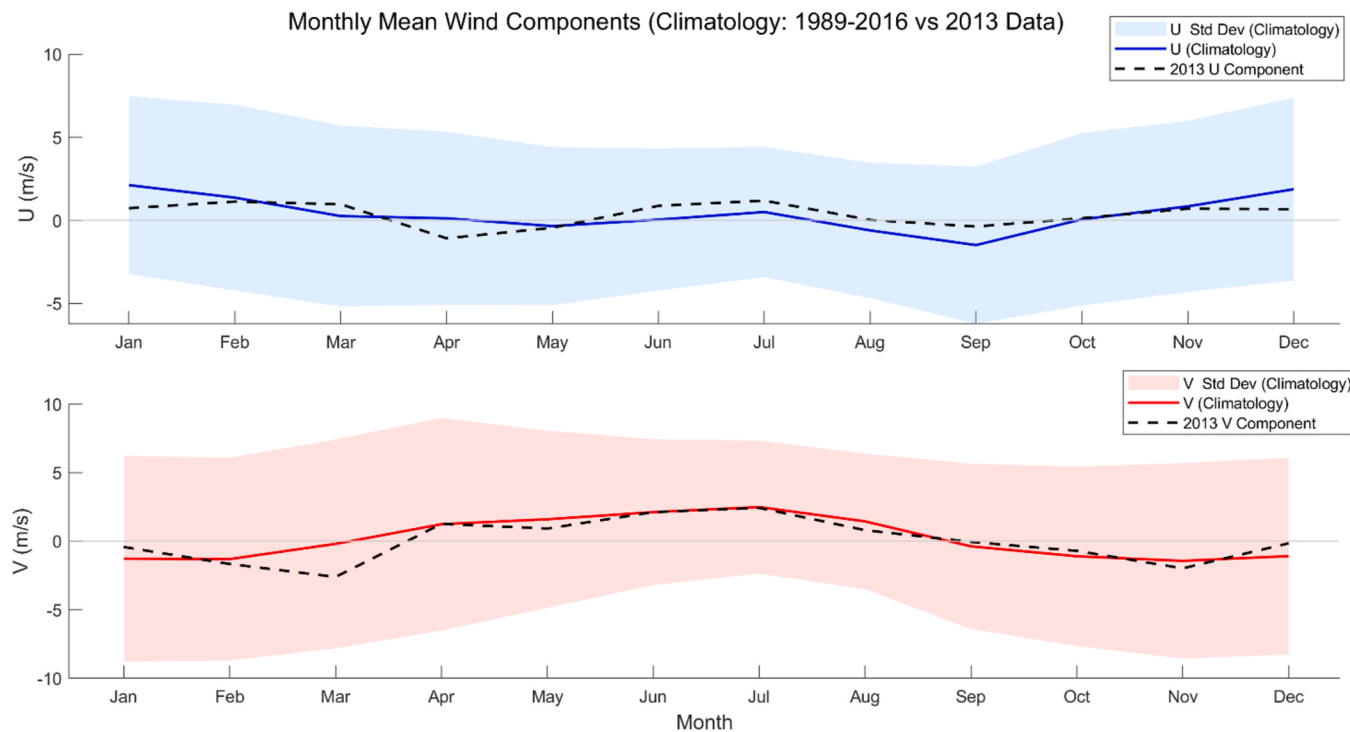


Fig. A.1. Comparison of 2013 monthly mean wind components with the 1989–2016 climatological averages. The top panel shows the zonal component (U , in blue), and the bottom panel shows the meridional component (V , in red). Shaded areas represent the climatological standard deviation, while black dashed lines correspond to the 2013 monthly mean wind components (U in the top panel, V in the bottom panel).

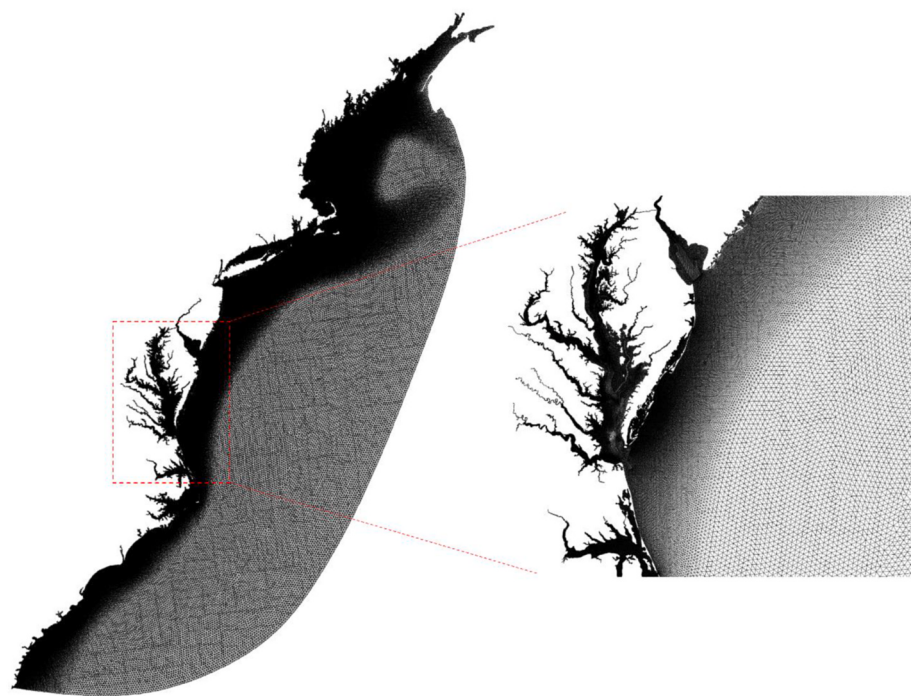


Fig. A.2. Grid domain of the US East Coast showing the unstructured grid. The inset highlights the finer resolution in the Chesapeake region, where particles were released.

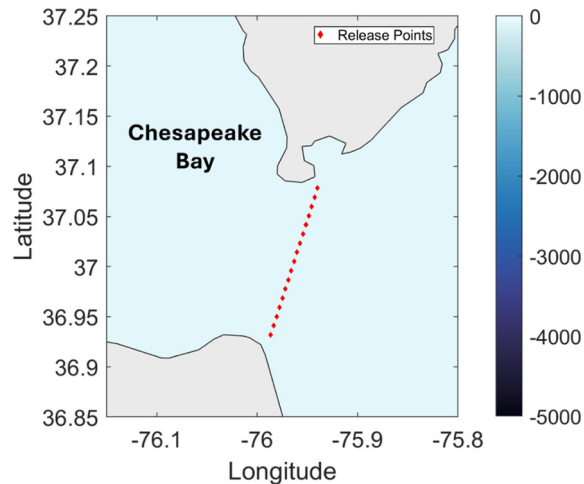


Fig. A.3. Particle release locations at the mouth of the Chesapeake Bay, spaced approximately 1 km apart and marked by red diamonds.

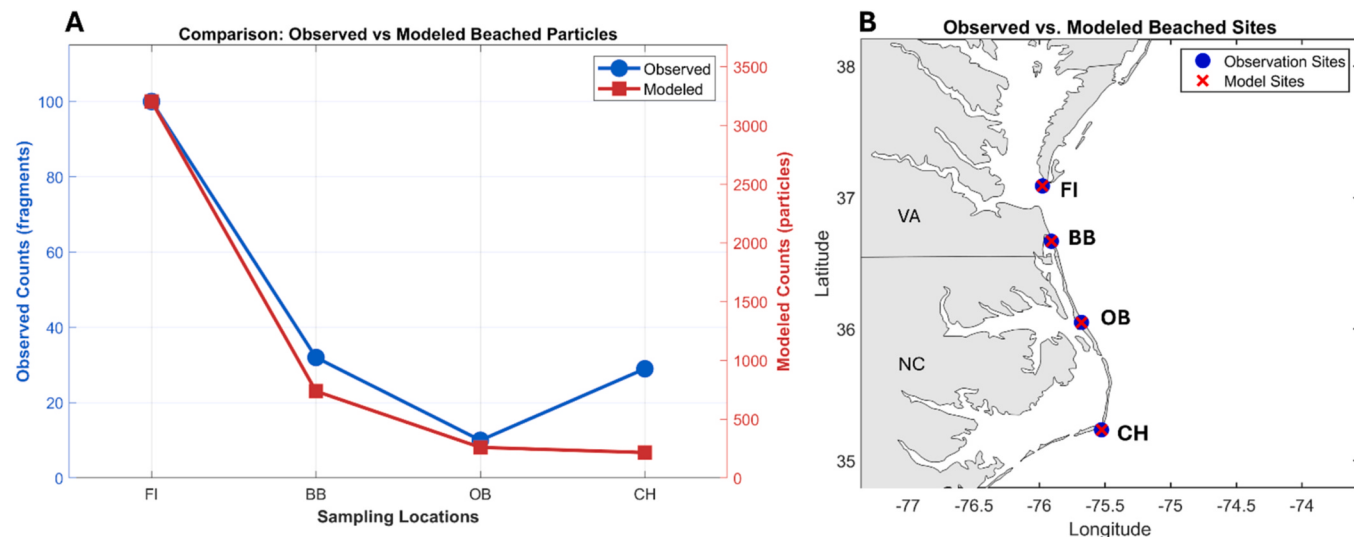


Fig. A.4. (A) Comparison of particle counts between observed microplastic fragments (blue) and biofouled modeled beached particles (orange) at four sampling sites: Fisherman Island (FI), Back Bay National Wildlife Refuge (BB), Outer Banks (OB), and Cape Hatteras National Seashore (CH). (B) Map showing the locations of observed sites (blue circles) and the nearest modeled points to the observations (red crosses) at the same four sampling locations (FI, BB, OB, CH).

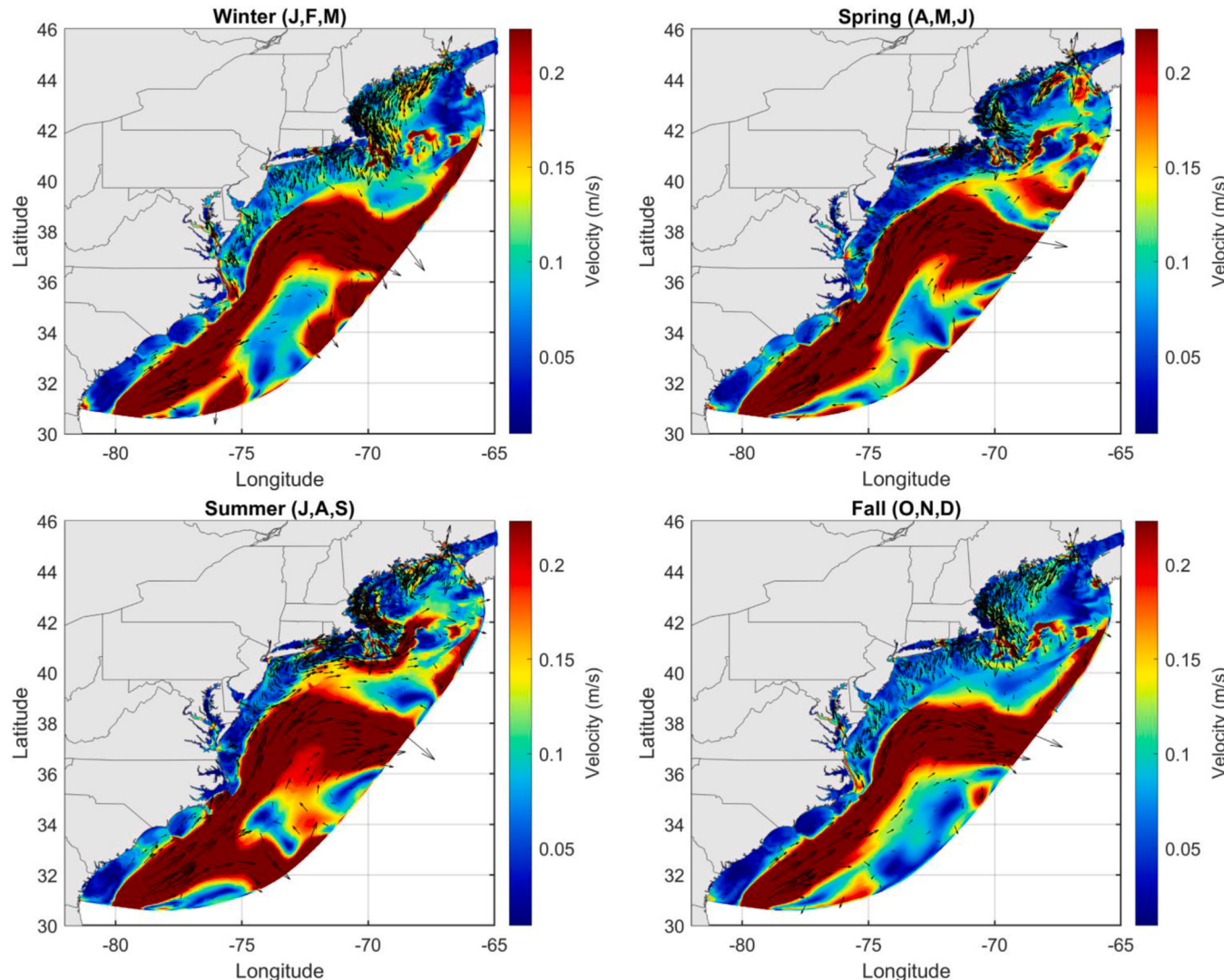


Fig. A.5. Mean surface currents by season for 2013: Winter (Jan–Mar), Spring (Apr–Jun), Summer (Jul–Sep), and Fall (Oct–Dec). The colorbar indicates current intensity (m/s), and vectors show the direction of the surface currents.

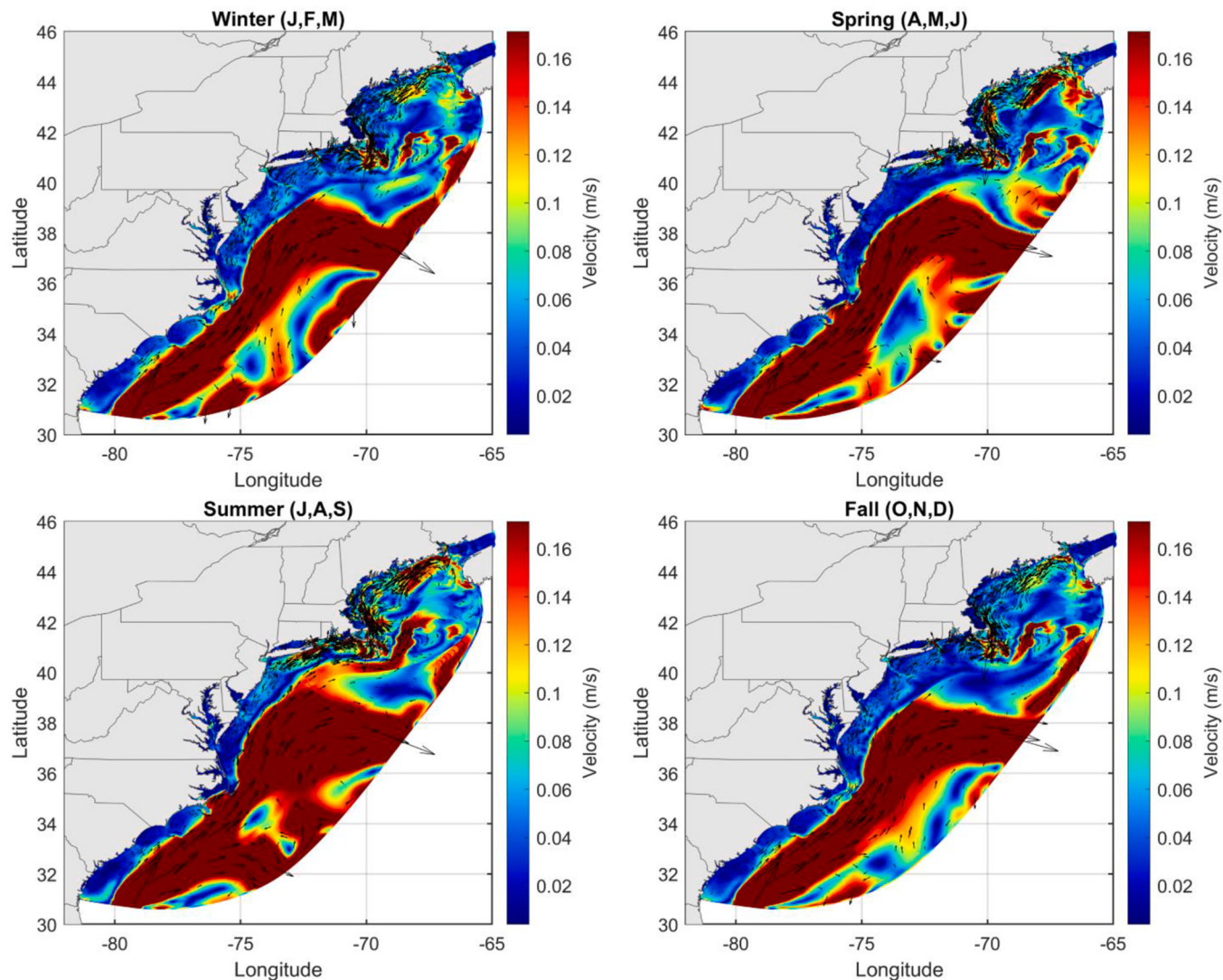


Fig. A.6. Mean subsurface currents by season for 2013: Winter (Jan–Mar), Spring (Apr–Jun), Summer (Jul–Sep), and Fall (Oct–Dec). The colorbar indicates current intensity (m/s), and vectors show the direction of the surface currents.

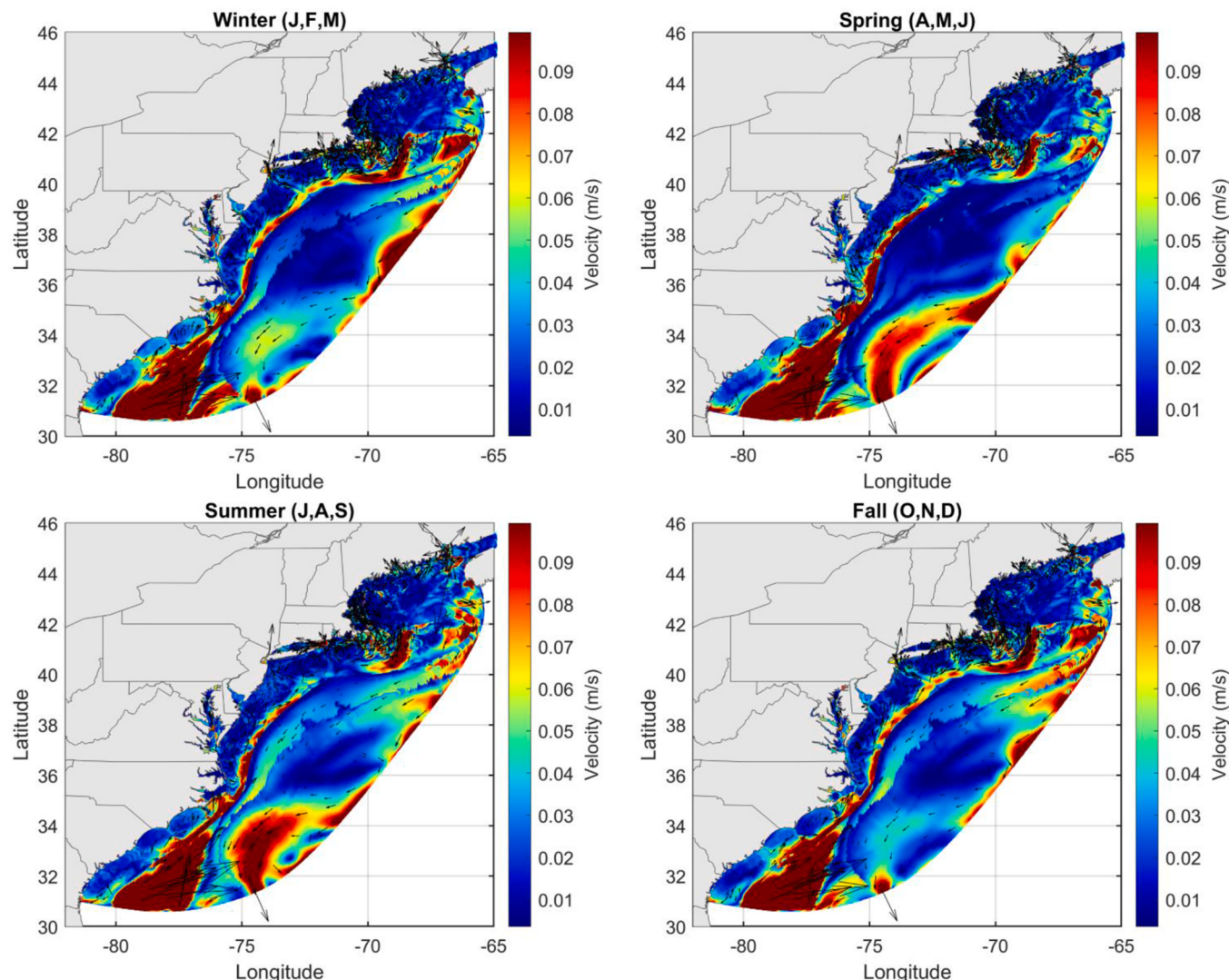


Fig. A.7. Mean near-bottom currents by season for 2013: Winter (Jan–Mar), Spring (Apr–Jun), Summer (Jul–Sep), and Fall (Oct–Dec). The colorbar indicates current intensity (m/s), and vectors show the direction of the bottom currents.

Data availability

Data will be made available on request.

References

- Akdogan, Z., Guven, B., 2019. Microplastics in the environment: a critical review of current understanding and identification of future research needs. *Environ. Pollut.* 254, 113011.
- Amaral-Zettler, L.A., Zettler, E.R., Mincer, T.J., Klaassen, M.A., Gallager, S.M., 2021. Biofouling impacts on polyethylene density and sinking in coastal waters: a macro/micro tipping point? *Water Res.* 201, 117289.
- Andrady, A.L., 2011. Microplastics in the marine environment. *Mar. Pollut. Bull.* 62 (8), 1596–1605.
- Arp, H.P.H., Kühnelt, D., Rummel, C., MacLeod, M., Potthoff, A., Reichelt, S., et al., 2021. Weathering plastics as a planetary boundary threat: exposure, fate, and hazards. *Environ. Sci. Technol.* 55 (11), 7246–7255.
- Besseling, E., Quik, J.T., Sun, M., Koelmans, A.A., 2017. Fate of nano-and microplastic in freshwater systems: a modeling study. *Environ. Pollut.* 220, 540–548.
- Browne, M.A., Dissanayake, A., Galloway, T.S., Lowe, D.M., Thompson, R.C., 2008. Ingested microscopic plastic translocates to the circulatory system of the mussel, *Mytilus edulis* (L.). *Environ. Sci. Technol.* 42 (13), 5026–5031.
- Cai, X., Qin, Q., Cui, L., Yang, X., Zhang, Y.J., Shen, J., 2025. NAAC (V1.0): a Seamless Two-Decade Cross-Scale Simulation from the North American Atlantic Coast to Tidal Wetlands Using the 3D unstructured-grid Model SCHISM (V5.11.0), 2025. EGUSphere, pp. 1–23.
- Chesapeake Bay Activities, 2019. Freshwater Flow into Chesapeake Bay. U.S. Geological Survey. Retrieved from. <https://www.usgs.gov/centers/chesapeake-bay-activities/science/freshwater-flow-chesapeake-bay>.
- Chiu, C.M., Huang, C.J., Wu, L.C., Zhang, Y.J., Chuang, L.Z.H., Fan, Y., Yu, H.C., 2018. Forecasting of oil-spill trajectories by using SCHISM and X-band radar. *Mar. Pollut. Bull.* 137, 566–581.
- Chiu, J.M.Y., Thiagarajan, V., Tsoi, M.Y.Y., Qian, P.Y., 2005. Qualitative and quantitative changes in marine biofilms as a function of temperature and salinity in summer and winter. *Biofilms* 2 (3), 183–195.
- Chubarenko, I., Bagaev, A., Zobkov, M., Esiukova, E., 2016. On some physical and dynamical properties of microplastic particles in marine environment. *Mar. Pollut. Bull.* 108 (1–2), 105–112.
- Chubarenko, I., Esiukova, E., Bagaev, A., Isachenko, I., Demchenko, N., Zobkov, M., et al., 2018. Behavior of microplastics in coastal zones. In: *Microplastic Contamination in Aquatic Environments*. Elsevier, pp. 175–223.
- Cohen, J.H., Internicola, A.M., Mason, R.A., Kukulka, T., 2019. Observations and simulations of microplastic debris in a tide, wind, and freshwater-driven estuarine environment: the Delaware Bay. *Environ. Sci. Technol.* 53 (24), 14204–14211.
- Costerton, J.W., 1995. Overview of microbial biofilms. *J. Ind. Microbiol. Biotechnol.* 15 (3), 137–140.
- Dodson, G.Z., Shotorbani, A.K., Hatcher, P.G., Waggoner, D.C., Ghosal, S., Noffke, N., 2020. Microplastic fragment and fiber contamination of beach sediments from selected sites in Virginia and North Carolina, USA. *Mar. Pollut. Bull.* 151, 110869.
- Du, J., Shen, J., 2016. Water residence time in Chesapeake Bay for 1980–2012. *J. Mar. Syst.* 164, 101–111.
- Eriksen, M., Lebreton, L.C., Carson, H.S., Thiel, M., Moore, C.J., Borerro, J.C., et al., 2014. Plastic pollution in the world's oceans: more than 5 trillion plastic pieces weighing over 250,000 tons afloat at sea. *PLoS One* 9 (12), e111913.

- Erni-Cassola, G., Zadjelevic, V., Gibson, M.I., Christie-Oleza, J.A., 2019. Distribution of plastic polymer types in the marine environment: A meta-analysis. *J. Hazard Mater.* 369, 691–698.
- Fazey, F.M., Ryan, P.G., 2016. Biofouling on buoyant marine plastics: an experimental study into the effect of size on surface longevity. *Environ. Pollut.* 210, 354–360.
- Ferguson, R.I., Church, M., 2004. A simple universal equation for grain settling velocity. *J. Sediment. Res.* 74 (6), 933–937.
- Fischer, M., Friedrichs, G., Lachnit, T., 2014. Fluorescence-based quasicontinuous and in situ monitoring of biofilm formation dynamics in natural marine environments. *Appl. Environ. Microbiol.* 80 (12), 3721–3728.
- Fisher, N.S., Bjerrregaard, P., Fowler, S.W., 1983. Interactions of marine plankton with transuranic elements. 1. Biokinetics of neptunium, plutonium, americium, and californium in phytoplankton. *Limnol. Oceanogr.* 28 (3), 432–447.
- Frias, J.P., Nash, R., 2019. Microplastics: finding a consensus on the definition. *Mar. Pollut. Bull.* 138, 145–147.
- Goodrich, D.M., 1988. On meteorologically induced flushing in three US east coast estuaries. *Estuar. Coast Shelf Sci.* 26 (2), 111–121.
- Gorman, D., Gutiérrez, A.R., Turra, A., Manzano, A.B., Balthazar-Silva, D., Oliveira, N.R., Harari, J., 2020. Predicting the dispersal and accumulation of microplastic pellets within the estuarine and coastal waters of South-Eastern Brazil using integrated rainfall data and Lagrangian particle tracking models. *Front. Environ. Sci.* 8, 559405.
- Hitchcock, J.N., 2020. Storm events as key moments of microplastic contamination in aquatic ecosystems. *Sci. Total Environ.* 734, 139436.
- Horton, A.A., Dixon, S.J., 2018. Microplastics: an introduction to environmental transport processes. *Wiley Interdiscip. Rev.: Water* 5 (2), e1268.
- Horton, A.A., Walton, A., Spurgeon, D.J., Lahive, E., Svendsen, C., 2017. Microplastics in freshwater and terrestrial environments: evaluating the current understanding to identify the knowledge gaps and future research priorities. *Sci. Total Environ.* 586, 127–141.
- Isobe, A., Kubo, K., Tamura, Y., Kako, S.I., Nakashima, E., Fujii, N., 2014. Selective transport of microplastics and mesoplastics by drifting in coastal waters. *Mar. Pollut. Bull.* 89 (1–2), 324–330.
- Iwasaki, S., Isobe, A., Kako, S.I., Uchida, K., Tokai, T., 2017. Fate of microplastics and mesoplastics carried by surface currents and wind waves: a numerical model approach in the Sea of Japan. *Mar. Pollut. Bull.* 121 (1–2), 85–96.
- Jalón-Rojas, I., Wang, X.H., Fredj, E., 2019. A 3D numerical model to Track Marine Plastic Debris (TrackMPD): sensitivity of microplastic trajectories and fates to particle dynamical properties and physical processes. *Mar. Pollut. Bull.* 141, 256–272.
- Jalón-Rojas, I., Sous, D., Marieu, V., 2025. A wave-resolving two-dimensional vertical Lagrangian approach to model microplastic transport in nearshore waters based on TrackMPD 3.0. *Geosci. Model Dev. (GMD)* 18 (2), 319–336.
- Jambeck, J.R., Geyer, R., Wilcox, C., Siegler, T.R., Perryman, M., Andrady, A., et al., 2015. Plastic waste inputs from land into the ocean. *Science* 347 (6223), 768–771.
- Karkanorachaki, K., Syranidou, E., Kalogerakis, N., 2021. Sinking characteristics of microplastics in the marine environment. *Sci. Total Environ.* 793, 148526.
- Kooi, M., Nes, E.H.V., Scheffer, M., Koelmans, A.A., 2017. Ups and downs in the ocean: effects of biofouling on vertical transport of microplastics. *Environ. Sci. Technol.* 51 (14), 7963–7971.
- Lebreton, L.C., Van Der Zwet, J., Damsteeg, J.W., Slat, B., Andrady, A., Reisser, J., 2017. River plastic emissions to the world's oceans. *Nat. Commun.* 8 (1), 15611.
- Lee, Y., Cho, J., Sohn, J., Kim, C., 2023. Health effects of microplastic exposures: current issues and perspectives in South Korea. *Yonsei Med. J.* 64 (5), 301.
- Lentz, S.J., Elgar, S., Guza, R.T., 2003. Observations of the flow field near the nose of a buoyant coastal current. *J. Phys. Oceanogr.* 33 (4), 933–943.
- Lentz, S.J., 2008a. Observations and a model of the mean circulation over the Middle Atlantic Bight continental shelf. *J. Phys. Oceanogr.* 38 (6), 1203–1221.
- Lentz, S.J., 2008b. Seasonal variations in the circulation over the Middle Atlantic Bight continental shelf. *J. Phys. Oceanogr.* 38 (7), 1486–1500.
- Liu, W.C., Tse, H.F., Fok, L., 2016. Plastic waste in the marine environment: a review of sources, occurrence and effects. *Sci. Total Environ.* 566, 333–349.
- Liu, K., Wang, X., Wei, N., Song, Z., Li, D., 2019. Accurate quantification and transport estimation of suspended atmospheric microplastics in megacities: implications for human health. *Environ. Int.* 132, 105127.
- Lobelle, D., Kooi, M., Koelmans, A.A., Laufkötter, C., Jongedijk, C.E., Kehl, C., Van Sebille, E., 2021. Global modeled sinking characteristics of biofouled microplastic. *J. Geophys. Res.: Oceans* 126 (4) e2020JC017098.
- López, A.G., Najjar, R.G., Friedrichs, M.A., Hickner, M.A., Wardrop, D.H., 2021. Estuaries as filters for riverine microplastics: simulations in a large, coastal-plain estuary. *Front. Mar. Sci.* 8, 715924.
- Malli, A., Corella-Puertas, E., Hajjar, C., Boulay, A.M., 2022. Transport mechanisms and fate of microplastics in estuarine compartments: a review. *Mar. Pollut. Bull.* 177, 113553.
- Mazzini, P.L., Chant, R.J., Scully, M.E., Wilkin, J., Hunter, E.J., Nidzieko, N.J., 2019. The impact of wind forcing on the thermal wind shear of a river plume. *J. Geophys. Res.: Oceans* 124 (11), 7908–7925.
- Moore, C., Guiguet, D., Dockins, C., Maguire, K.B., Simon, N.B., 2018. Valuing ecological improvements in the Chesapeake Bay and the importance of ancillary benefits. *J. Benefit-Cost Anal.* 9 (1), 1–26.
- Plastic Europe, 2024. The circular economy for plastics: a European analysis. <https://plasticseurope.org/knowledge-hub/the-circular-economy-for-plastics-a-european-analysis-is-2024/>.
- Politikos, D.V., Ioakeimidis, C., Papatheodorou, G., Tsiaras, K., 2017. Modeling the fate and distribution of floating litter particles in the Aegean Sea (E. Mediterranean). *Front. Mar. Sci.* 4, 191.
- Politikos, D.V., Tsiaras, K., Papatheodorou, G., Anastasopoulou, A., 2020. Modeling of floating marine litter originated from the Eastern Ionian Sea: transport, residence time and connectivity. *Mar. Pollut. Bull.* 150, 110727.
- Pothiraj, C., Gokul, T.A., Kumar, K.R., Ramasubramanian, A., Palanichamy, A., Venkatachalam, K., et al., 2023. Vulnerability of microplastics on marine environment: a review. *Ecol. Indic.* 155, 111058.
- Qin, Q., Shen, J., Tuckey, T.D., Cai, X., Xiong, J., 2022. Using forward and backward particle tracking approaches to analyze impacts of a water intake on Ichthyoplankton mortality in the appomattox River. *J. Mar. Sci. Eng.* 10 (9), 1299.
- Roarty, H., Glenn, S., Brodie, J., Nazzaro, L., Smith, M., Handel, E., et al., 2020. Annual and seasonal surface circulation over the Mid-Atlantic Bight Continental Shelf derived from a decade of high frequency radar observations. *J. Geophys. Res.: Oceans* 125 (11) e2020JC016368.
- Rochman, C.M., Brookson, C., Bikker, J., Djuric, N., Earn, A., Bucci, K., et al., 2019. Rethinking microplastics as a diverse contaminant suite. *Environ. Toxicol. Chem.* 38 (4), 703–711.
- Seim, H.E., Savidge, D., Andres, M., Bane, J., Edwards, C., Gawarkiewicz, G., et al., 2022. Overview of the processes driving exchange at Cape Hatteras program. *Oceanography (Wash. D. C.)* 35 (2).
- Sousa, M.C., DeCastro, M., Gago, J., Ribeiro, A.S., Des, M., Gómez-Gesteira, J.L., et al., 2021. Modelling the distribution of microplastics released by wastewater treatment plants in Ria de Vigo (NW Iberian Peninsula). *Mar. Pollut. Bull.* 166, 112227.
- Sun, Y., Cao, L., Wang, Y., Chen, W., Li, Y., Zhao, X., 2022. Sources and distribution of microplastics in the east China sea under a three-dimensional numerical modelling. *Environ. Pollut.* 311, 119910.
- Tsiaras, K., Hatzoniakakis, Y., Kalaroni, S., Pollani, A., Triantafyllou, G., 2021. Modeling the pathways and accumulation patterns of micro-and macro-plastics in the Mediterranean. *Front. Mar. Sci.* 8, 743117.
- Uzun, P., Farazande, S., Guven, B., 2022. Mathematical modeling of microplastic abundance, distribution, and transport in water environments: a review. *Chemosphere* 288, 132517.
- Van Melkebeke, M., Janssen, C., De Meester, S., 2020. Characteristics and sinking behavior of typical microplastics including the potential effect of biofouling: implications for remediation. *Environ. Sci. Technol.* 54 (14), 8668–8680.
- Vercauteran, M., Lambert, S., Hoogerwerf, E., Janssen, C.R., Asselman, J., 2024. Microplastic-specific biofilm growth determines the vertical transport of plastics in freshwater. *Sci. Total Environ.* 910, 168399.
- Yonkos, L.T., Friedel, E.A., Perez-Reyes, A.C., Ghosal, S., Arthur, C.D., 2014. Microplastics in four estuarine rivers in the Chesapeake Bay, USA. *Environ. Sci. Technol.* 48 (24), 14195–14202.
- Zhao, S., Mincer, T.J., Lebreton, L., Egger, M., 2023. Pelagic microplastics in the North Pacific Subtropical Gyre: a prevalent anthropogenic component of the particulate organic carbon pool. *PNAS Nexus* 2 (3) pgad070.
- Zhang, Y., Baptista, A.M., 2008. SELFIE: a semi-implicit Eulerian-Lagrangian finite-element model for cross-scale ocean circulation". *Ocean Model.* 21 (3–4), 71–96.
- Zhang, Y., Kang, S., Allen, S., Allen, D., Gao, T., Sillanpää, M., 2020. Atmospheric microplastics: a review on current status and perspectives. *Earth Sci. Rev.* 203, 103118.
- Zhang, Y., Ye, F., Stanev, E.V., Grashorn, S., 2016. Seamless cross-scale modeling with SCHISM. *Ocean Model.* 102, 64–81.
- Zhang, Z., Wu, H., Peng, G., Xu, P., Li, D., 2020. Coastal ocean dynamics reduce the export of microplastics to the open ocean. *Sci. Total Environ.* 713, 136634.